Select α-arrestins control cell-surface abundance of the mammalian Kir2.1 potassium channel in a yeast model

Received for publication, December 5, 2017, and in revised form, May 4, 2018 Published, Papers in Press, May 21, 2018, DOI 10.1074/jbc.RA117.001293

Natalie A. Hager[‡], Collin J. Krasowski[‡], Timothy D. Mackie[§], Alexander R. Kolb[§], Patrick G. Needham[§], Andrew A. Augustine[§], Alison Dempsey[¶], Christopher Szent-Gyorgyi[¶], Marcel P. Bruchez[¶], Daniel J. Bain[‖], Adam V. Kwiatkowski[**], Allyson F. O'Donnell[‡1], and Jeffrey L. Brodsky[§2]

From the [‡]Department of Biological Sciences, Duquesne University, Pittsburgh, Pennsylvania 15282, the [§]Department of Biological Sciences, University of Pittsburgh, Pittsburgh, Pennsylvania 15260, the [¶]Molecular Biosensor and Imaging Center, Carnegie Mellon University, Pittsburgh, Pennsylvania 15213, the [‖]Department of Geology and Environmental Sciences, University of Pittsburgh, Pittsburgh, Pennsylvania 15260, and the [**]Department of Cell Biology, University of Pittsburgh School of Medicine, Pittsburgh, Pennsylvania 15261

Edited by Ursula Jakob

Protein composition at the plasma membrane is tightly regulated, with rapid protein internalization and selective targeting to the cell surface occurring in response to environmental changes. For example, ion channels are dynamically relocalized to or from the plasma membrane in response to physiological alterations, allowing cells and organisms to maintain osmotic and salt homeostasis. To identify additional factors that regulate the selective trafficking of a specific ion channel, we used a yeast model for a mammalian potassium channel, the K^+ inward rectifying channel Kir2.1. Kir2.1 maintains potassium homeostasis in heart muscle cells, and Kir2.1 defects lead to human disease. By examining the ability of Kir2.1 to rescue the growth of yeast cells lacking endogenous potassium channels, we discovered that specific α-arrestins regulate Kir2.1 localization. Specifically, we found that the Ldb19/Art1, Aly1/Art6, and Aly2/Art3 α-arrestin adaptor proteins promote Kir2.1 trafficking to the cell surface, increase Kir2.1 activity at the plasma membrane, and raise intracellular potassium levels. To better quantify the intracellular and cell-surface populations of Kir2.1, we created fluorogen-activating protein fusions and for the first time used this technique to measure the cell-surface residency of a plasma membrane protein in yeast. Our experiments revealed that two α-arrestin effectors also control Kir2.1 localization. In particular, both the Rsp5 ubiquitin ligase and the protein phosphatase calcineurin facilitated the α-arrestin–mediated trafficking of Kir2.1. Together, our findings implicate α-arrestins in regulating an additional class of plasma membrane proteins and establish a new tool for dissecting the trafficking itinerary of any membrane protein in yeast.

All eukaryotic cells continually alter the complement of proteins at the cell surface and in intracellular membranes to reflect changing demands on cellular function. Membrane protein redistribution to the cell surface requires that protein trafficking pathways respond to these demands. In many cases, membrane proteins must be selectively packaged into secretory vesicles that transit from one location to another based on their specific function. These intricate changes in protein trafficking and activity are essential on a continual basis in muscle cells and especially in cardiac myocytes, where with every beat of the contracting heart ion channels, transporters, and hormone receptors must be appropriately positioned to ensure proper function. Despite this central role of regulated protein trafficking in muscle function, we know relatively little about regulated protein trafficking in contractile systems, in part because of the inherent difficulties of working in these systems (1, 2).

To begin to identify regulators of ion channel trafficking that may facilitate cardiac function, we previously employed a yeast model in which a mammalian potassium channel, Kir2.1, was ectopically expressed (3). Kir2.1 is encoded by the *KCNJ2* gene and is a member of the family of K^+ inward rectifying (Kir)[3] 2 channels. Kir2.1, one of five members of the Kir family that are expressed in heart, skeletal muscle, and neurons, restores and maintains membrane potential after muscle contraction (4, 5). Functional Kir channels are homotetrameric, and each subunit contains two transmembrane spans (6). When the tetramer assembles, which is thought to occur soon after its synthesis on endoplasmic reticulum (ER)–associated ribosomes (6, 7), a potassium-selective pore is generated. Consistent with a role in

This work was supported, in whole or in part, by National Institutes of Health Grants R01 HL127711 (to A. V. K.), R01 GM075061 (to J. L. B. and A. F. O.), P30 DK079307 (to J. L. B.), and U54-GM103529 (to A. D., C. S.-G., and M. P. B). This work also was supported by National Science Foundation (NSF) MCB CAREER Grant 1553143 (to A. F. O.) and NSF EAR-IF 0948366 (to D. J. B.), a Pilot Grant from P30 DK079307 (to A. F. O.), and a grant from the Shurl and Kay Curci Foundation (to M. P. B.). The authors declare that they have no conflicts of interest with the contents of this article. The content is solely the responsibility of the authors and does not necessarily represent the official views of the National Institutes of Health.

This article contains Figs. S1 and S2, Table S1, and additional references.

[1] To whom correspondence may be addressed: Dept. of Biological Sciences, Duquesne University, 600 Forbes Ave., Pittsburgh, PA 15282. Tel.: 412-396-4356; E-mail: odonne15@duq.edu.

[2] To whom correspondence may be addressed: Dept. of Biological Sciences, University of Pittsburgh, Pittsburgh, PA 15260. Tel.: 412-624-4831; E-mail: jbrodsky@pitt.edu.

[3] The abbreviations used are: Kir, K^+ inward rectifying; ER, endoplasmic reticulum; ICP-MS, inductively coupled plasma mass spectrometry; FAP, fluorogen-activating protein; MVB, multivesicular body; ESCRT, endosomal sorting complexes required for transport; SCA, single-chain antibody; MG, malachite green; LatA, latrunculin A; a.u., arbitrary units; TM, transmembrane; AzC, azetidine-2-carboxylic acid; GST, glutathione *S*-transferase; SC, synthetic complete.

cardiac myocyte membrane repolarization, gain-of-function or loss-of-function mutations in Kir2.1 cause short or long QT syndromes, respectively, which result in cardiac arrhythmias (8, 9). For example, loss-of-function mutations that reduce Kir2.1 activity at the cell surface lead to Andersen–Tawil syndrome (8, 10, 11). Moreover, several of the disease-causing *KCNJ2* alleles are associated with defects in Kir2.1 trafficking. T192A diminishes Kir2.1 binding to plasma membrane phosphatidylinositol 4,5 bisphosphate (PIP_2), reducing channel opening at the cell surface (12), and deletion of amino acids 314–315 abrogates Kir2.1 binding to the clathrin adaptin complex 1 (AP-1), which delivers the channel to the plasma membrane from the trans-Golgi complex (13). Other studies indicate that the regulated exocytosis of Kir2.1 from intracellular stores is critical to maintain Kir2.1 activity at the cell surface (13–15).

Consistent with the importance of protein trafficking in the late secretory pathway, we reported that ESCRT regulates Kir2.1 activity at the cell surface in both yeast and mammalian cells (3). The yeast system relies on the ability of an exogenous potassium channel to rescue the growth of yeast lacking two endogenous potassium channels (*TRK1* and *TRK2*) on low-potassium medium (16), and mutations in genes encoding ESCRT components augment growth under these selective conditions (3). However, we were unable to demonstrate directly that mutations in these trafficking complexes increase the amount of Kir2.1 at the plasma membrane. Furthermore, it is likely that other regulators of the secretory pathway contribute to channel trafficking, because the identification of ESCRT and additional components was undertaken by analyzing the yeast deletion collection. Therefore, functionally redundant factors that contribute to Kir2.1 trafficking were most likely missed when the deletion collection was screened.

Here, we used a targeted screen to reveal the role of α-arrestins in regulating Kir2.1 trafficking in yeast. The α-arrestins are a class of conserved protein adaptors that link specific cargo proteins to a ubiquitin ligase, known as Rsp5, and facilitate protein sorting in the late secretory pathway (17–22). From this screen, we determined that three α-arrestins, Aly1, Aly2, and Ldb19 (also known as Art6, Art3, and Art1), promote Kir2.1-dependent growth of yeast on low-potassium medium. To show directly that the overexpression of the α-arrestins increases Kir2.1 residence at the plasma membrane, we implemented an imaging technology that employs a fluorogen-activating protein (FAP) fusion to Kir2.1. Although this FAP reporter was first developed in yeast (23), surprisingly it has not been used to detect the residence of membrane proteins at the cell surface in this organism. Instead, it has been applied only to monitor protein trafficking in mammalian cells (24, 25). As hypothesized, we were able to demonstrate that Ldb19, Aly1, and Aly2 increase the cell-surface pool of Kir2.1, which they do by increasing Kir2.1 delivery to the plasma membrane rather than by reducing Kir2.1 endocytic turnover. Furthermore, our genetic studies indicated that the Rsp5 E3 ubiquitin ligase is required for α-arrestin–mediated trafficking of Kir2.1 to the cell surface and that phosphoregulation of Aly1 also plays important roles during this process. Together, our findings pave the way for future investigations of α-arrestin regulation of Kir2.1 in human cells, expand the role of α-arrestins in regulating the residence of specific protein cargo, and demonstrate the general applicability of a new fluorescence imaging technology that can detect the levels of low abundance proteins at the yeast plasma membrane.

Results

A targeted screen identifies select α-arrestins as Kir2.1 regulators

The localization of the Kir2.1 potassium channel is tightly regulated to ensure the maintenance of potassium homeostasis in cardiac and other cells (8, 9, 13). Defects in protein quality control and trafficking pathways that govern Kir2.1 activity have clinical consequences (8, 9, 13). For example, mutation of Kir2.1, which abrogates its association with AP-1, a clathrin adaptor required for Golgi-to-plasma membrane trafficking, blunts Kir2.1 targeting to the plasma membrane and leads to Andersen–Tawil syndrome, which causes ventricular arrhythmias (13). To define the protein trafficking and quality control pathways that regulate Kir2.1, we used a system developed previously by our group to uncover the regulators of Kir2.1 surface activity (3). Specifically, we utilized the fact that the expression of an exogenous potassium transporter, such as Kir2.1, restores the growth of yeast lacking two endogenous potassium transporters, *TRK1* and *TRK2*, on low-potassium medium (3, 16, 26, 27). In this system, a growth defect is evident when *trk1*Δ *trk2*Δ cells are incubated on medium supplemented with either 25 or 10 mM KCl (Fig. S1*A*; and see Fig. 1*A*, *panel* with pRS426 vector), but improved growth is evident on 25 mM KCl only when yeast express Kir2.1 (Fig. S1*A* and Ref. 3). These data strongly suggested that Kir2.1 forms a functional potassium transporter when expressed in yeast and elevates intracellular potassium. However, it is possible that the expression of an exogenous protein leads to a stress response, allowing cells to grow on low-KCl medium through an unidentified pathway. Therefore, to validate this system, we first assessed intracellular potassium levels using inductively coupled plasma mass spectrometry (ICP-MS) analyses after cells had been grown for 6–8 h in low-potassium medium. ICP-MS allows for total intracellular element composition to be determined. By using this technique, we found that *trk1*Δ *trk2*Δ cells had ~40% less cellular potassium than their WT counterparts, but ectopic expression of mammalian Kir2.1 in *trk1*Δ *trk2*Δ cells increased intracellular potassium by ~20%, (Fig. 1*B*). In contrast, the expression of Kir2.1-AAA, in which amino acids ^{144}GYG^{146} of the potassium selectivity filter within Kir2.1 are mutated to Ala (3, 28), failed to increase intracellular potassium levels compared with the vector control (Fig. 1*B*). This mutant was also unable to improve growth on low-potassium medium (see below), even though the protein is expressed at similar levels to WT Kir2.1 (3). From these analyses, we show for the first time that the heterologous expression of the Kir2.1 potassium channel in *trk1*Δ *trk2*Δ yeast directly increases intracellular potassium.

Although our earlier systematic screen identified multiple regulators of Kir2.1 in the yeast model, including components of the ESCRT pathway (3), one caveat was that only single-gene deletions were examined. Therefore, a gene whose function is redundant with that of a second gene would have been missed.

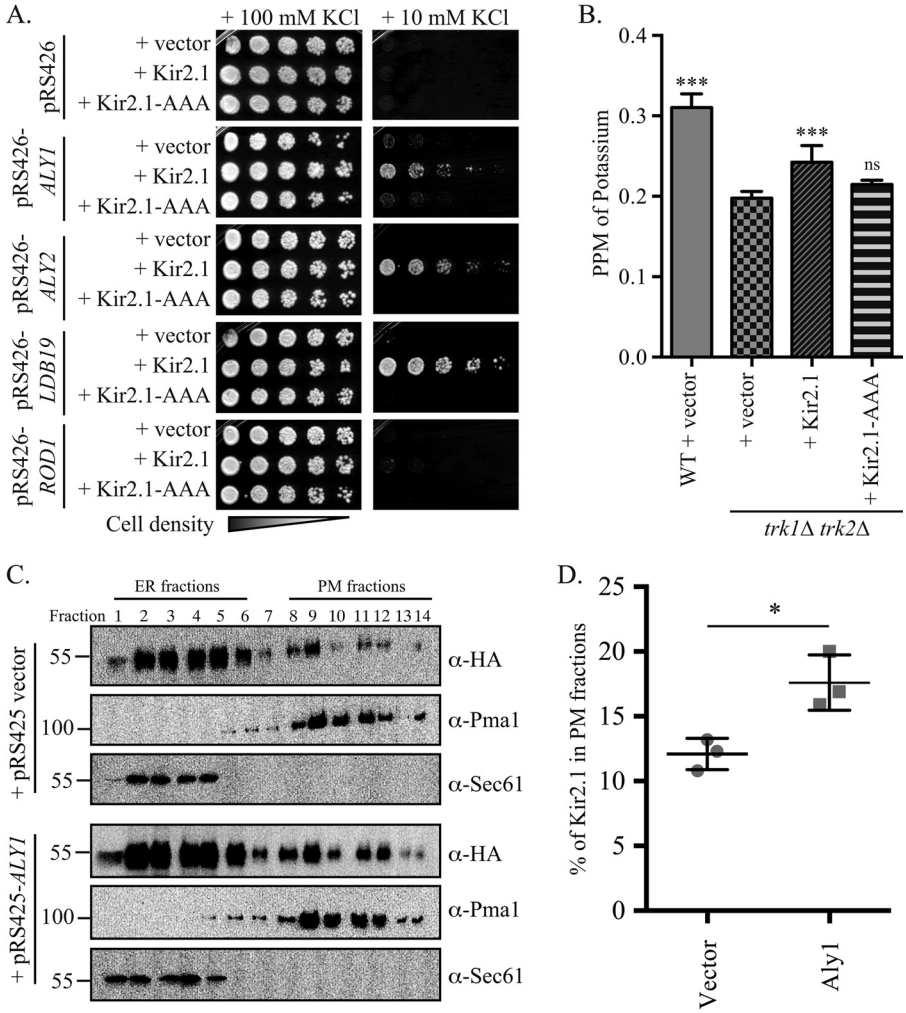

Figure 1. α-Arrestins Aly1, Aly2, and Ldb19 promote Kir2.1-dependent growth on low-potassium medium. *A*, growth of serial dilutions of *trk1*Δ *trk2*Δ cells containing the indicated plasmids on SC medium lacking uracil and leucine and containing the indicated added concentrations of KCl is shown after 2 days. *B*, WT (BY4741) or *trk1*Δ *trk2*Δ cells containing the indicated plasmids were grown in 10 mM KCl-containing medium, and then cellular potassium levels were measured using ICP-MS. The ppm of KCl for an equivalent number of cells was determined for four replicates, and the mean ± S.D. was calculated (presented as *error bars*). Pairwise Student's *t* tests were performed to assess significance (***, $p < 0.0001$; *ns*, $p > 0.01$, not significant) relative to *trk1*Δ *trk2*Δ cells with the vector control. *C*, lysates from cells expressing Kir2.1 and a vector control or overexpressing Aly1 were analyzed by sucrose gradient density fractionation (30–70%) under conditions to optimize separation of the ER and plasma membrane (*PM*) fractions. Fractions 1 and 14 are at the *top* and *bottom* of the gradient, respectively. Immunoblot analyses were used to detect Kir2.1 (α-HA antibody), ER-resident protein Sec61, and the plasma membrane protein Pma1. One of three representative experiments is shown. *D*, the percentage of total Kir2.1 signal in the plasma membrane (fractions 8–14) was quantified using ImageJ for three replicate sucrose gradients; the mean percent signal ± S.D. are presented along with the individual data points for each replicate. A Student's *t* test was performed to assess significance (*, $p < 0.01$).

Consequently, we adopted a targeted screening approach in which we selectively overexpressed functionally redundant factors in Kir2.1-expressing *trk1*Δ *trk2*Δ yeast. Growth on low-potassium medium was then measured to identify members of the corresponding gene family that might regulate Kir2.1 trafficking. As a first proof of principle for this analysis, we chose the α-arrestin–trafficking adaptors because: 1) α-arrestins are important for the selective trafficking of a wide array of integral membrane cargo proteins, from G protein–coupled receptors to nutrient permeases and metal transporters (17–21), demonstrating their functional plasticity; 2) α-arrestins can act in a functionally redundant manner such that multiple α-arrestins may regulate the localization of a single membrane cargo protein, making it likely that these genes would have been missed in our initial screen (17, 19, 20); 3) α-arrestins can regulate both intracellular sorting and endocytosis (18–20, 29–32), indicating that Kir2.1 localization can be affected through more than one route; and 4) α-arrestins are conserved from yeast to man (33), suggesting that the results of our study have the potential to define previously unknown regulators of Kir2.1 in mammalian cells.

We overexpressed 12 of the 14 known yeast α-arrestins in *trk1*Δ *trk2*Δ cells constitutively expressing Kir2.1 or the Kir2.1-AAA potassium channel mutant (3, 28) as a negative control (Figs. 1*A* and S1*B*). In this experiment, yeast containing an empty vector provided another control, and in all cases growth was essentially identical between the vector and Kir2.1-AAA–expressing cells. In contrast, overexpression of one of three α-arrestins, Aly1, Aly2, and Ldb19, strongly improved growth on low-potassium medium when Kir2.1 was expressed, but their expression had no effect on the growth of cells containing the vector control or the Kir2.1-AAA mutant (Fig. 1*A*). Addi-

tionally, ICP-MS analyses demonstrated that overexpression of Aly1, Aly2, and Ldb19 significantly increased intracellular potassium levels compared with the vector control (see below). Four of the other α-arrestins tested (Bul2, Rog3, Art5, and Rim8) modestly improved growth on low potassium, whereas the other five α-arrestins tested (Rod1, Bul1, Bul2, Ecm21, Csr2, and Art10) showed no improvement of growth on low-potassium medium (Fig. S1*B*). Based on these data, we suggest that Aly1, Aly2, and Ldb19 promote Kir2.1 activity and/or localization at the plasma membrane, and we chose these three α-arrestins as the focus of further study.

Previously, we used indirect immunofluorescence microscopy and biochemical fractionation experiments to determine that most Kir2.1 is retained in the ER and only a small pool of total Kir2.1 reaches the plasma membrane (3). These data align with the fact that the screen for growth on low potassium is quite sensitive and that Kir2.1 exhibits a high open probability (5, 16, 26, 34), so only a small population of cell surface–resident protein is needed for growth. Nevertheless, we fractionated *trk1*Δ *trk2*Δ cells expressing Kir2.1 that either contained a vector control or overexpressed *ALY1*. After sucrose gradient density centrifugation, we resolved the ER and plasma membrane–enriched fractions and examined Kir2.1 residence (Fig. 1*C*). Consistent with our previous study, the majority of Kir2.1 co-migrated with the Sec61-marked ER fractions (Fig. 1*C*, fractions 1–6), and only ~12% of Kir2.1 co-migrated with the Pma1-marked plasma membrane fractions (fractions 8–14) when lysates from cells containing the vector control were examined (Fig. 1, *C* and *D*). However, in extracts from cells overexpressing *ALY1*, the amount of Kir2.1 co-migrating with the Pma1-marked plasma membrane fractions (fractions 8–14) rose significantly when gradients from three independent experiments were analyzed (Fig. 1, *C* and *D*). This increase in the plasma membrane fraction of Kir2.1 in cells overexpressing Aly1 is not because of an overall elevated abundance of Kir2.1 in the cell. Specifically, when whole-cell extracts were examined by immunoblotting, overexpression of Aly1, Aly2, or Ldb19 did not significantly alter Kir2.1 abundance compared with the vector control (Fig. S1*C*). Taken together, these data support a model in which the overexpression of select α-arrestins promotes Kir2.1 trafficking to the plasma membrane, thereby increasing intracellular potassium. Although this function is counter to the more frequently reported role of α-arrestins in regulating the endocytosis of plasma membrane proteins, the results are consistent with other studies showing that α-arrestins can also play important roles in intracellular protein sorting and recycling (29, 30, 35, 36).

FAP-tagged Kir2.1 measures surface channel abundance

We next sought to better characterize Kir2.1 residence in cells overexpressing *ALY1*, *ALY2*, or *LDB19*. However, the large fraction of ER-localized Kir2.1 occludes analyses of the plasma membrane pool of Kir2.1, which is of low abundance, when using traditional imaging approaches. We therefore implemented an alternate strategy that employs a fluorogen-activating protein. This strategy was first described by Waggoner and co-workers (37) and makes use of single-chain antibodies (SCA) selected for their ability to bind to nonfluorescent malachite green (MG)–derived dyes (Fig. 2*A*). Neither the SCA nor the MG-derived dye fluoresce in solution, but when the dye binds the SCA, a >10,000-fold increase in fluorescence is detected (23, 38). Under these conditions, the SCA and the MG-derived dye comprise a FAP pair. Moreover, by using a cell-permeant form of the dye (referred to hereafter as MG-ESTER), or a cell-impermeant form of the dye (referred to hereafter as MG-B-TAU), the localization of the total cellular pool *versus* the plasma membrane–resident pool of the fusion protein can be detected and quantified (Fig. 2*B*). Although the dye-binding SCA modules were first identified in yeast (23, 37, 38), this technology has not been used to monitor the cellular residence of proteins expressed in this model organism.

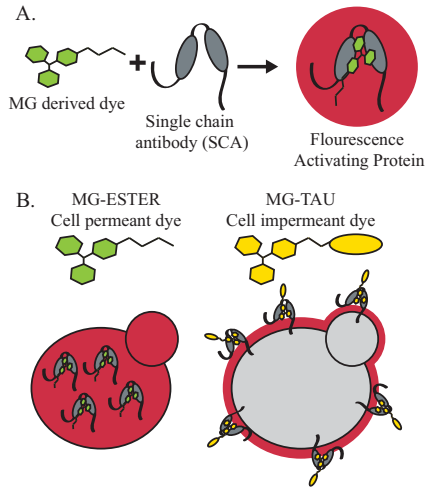

Figure 2. The use of a fluorogen-activating protein to report on cellular residence. *A*, the FAP technique makes use of a MG-derived dye that binds an SCA. Neither the MG nor the SCA is fluorescent, but when the MG dye is bound by an SCA, fluorescence is detected. *B*, the MG-derived dye can be conjugated to a membrane-soluble side chain (MG-ESTER, cell-permeant dye) that freely passes through the yeast cell wall and the plasma membrane, where it can be bound by intracellular SCAs to activate fluorescence and monitor the intracellular levels of a tagged protein. The MG-derived dye can also be conjugated to a membrane-impermeant side chain, as is the case with the MG-B-TAU dye. This dye can no longer enter the cell, so only the SCAs on the external face of the cell surface will be bound by dye and fluoresce.

To make use of the cell-excluded dye, the FAP tag must reside on the extracellular side of the plasma membrane. Because both the N- and C termini of Kir2.1 are cytosolic (6), we appended an N-terminal transmembrane (TM) domain to Kir2.1 and inserted the FAP tag upstream of the TM. This generated FAP-TM-Kir2.1, which positions the FAP tag in the extracellular space where it will be accessible to MG-B-TAU (Fig. 3*A*). We then placed the gene encoding this fusion protein under the control of the strong, constitutive *TEF1* promoter. To verify that the MG-B-TAU dye was cell-impermeant in yeast and thus unable to activate the fluorescence of the intracellular pool of Kir2.1, we generated plasmids expressing C-terminal FAP-tagged versions of Sec61 and Sec63 from the constitutive *TEF1* promoter. Sec61 and Sec63 are components of the protein translocation machinery in the yeast ER and stably reside in this compartment (39). Next, the FAP-TM-Kir2.1, Sec61-TM, and Sec63-TM expression plasmids were transformed into *trk1*Δ *trk2*Δ cells and imaged by confocal microscopy after a 30-min incubation with either the cell-permeant (MG-ESTER) or cell-impermeant (MG-B-TAU) dyes. As antic-

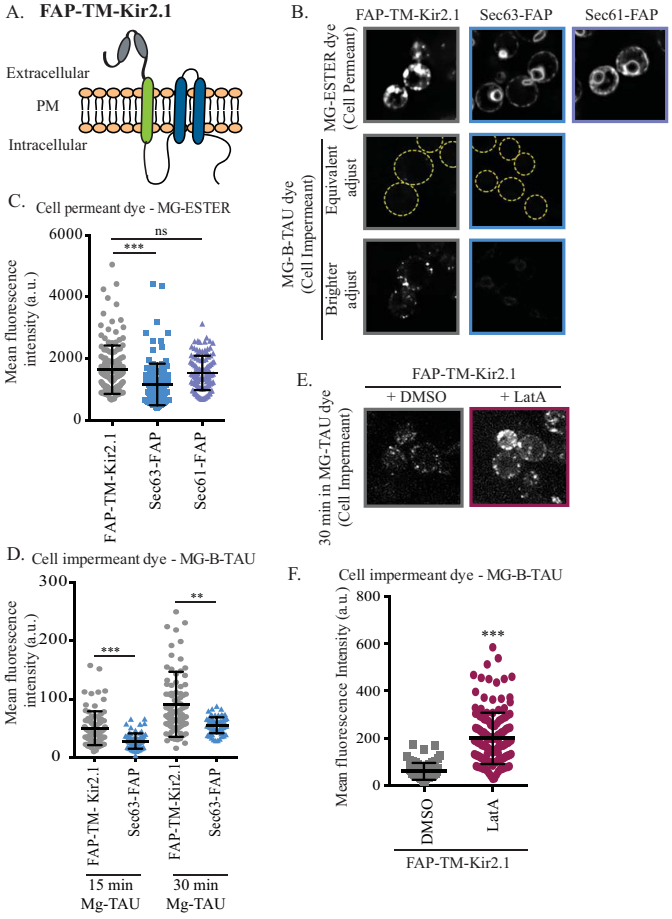

Figure 3. FAP-tagged Kir2.1 can be detected at the cell surface. *A*, schematic of FAP-tagged Kir2.1. Kir2.1 transmembrane domains are shown in *blue*, and the platelet-derived growth factor transmembrane domain is shown in *green*. The FAP tag extends from the N terminus and is shown as *gray ovals*. *B*, cells expressing FAP-TM-Kir2.1, Sec63-FAP, or Sec61-FAP were incubated with the MG-ESTER or MG-B-TAU dye to activate intracellular or cell-surface FAP-tag fluorescence, respectively. Confocal microscopy images of medial sections of cells incubated with dye for 30 min are shown. In the *top two rows*, cells are adjusted equivalently to show that the signal from intracellular FAP-TM-Kir2.1 or Sec63-FAP is lost when the MG-B-TAU dye is used. *Yellow dashed-line circles* are used in the *second row* to demark the cell. The *bottom row* of images are the same images as shown in the second row but are adjusted to allow the cell-surface fluorescence of the MG-B-TAU–stained FAP-TM-Kir2.1–expressing cells to be seen. *C* and *D*, total cellular fluorescence for $n > 70$ cells, imaged as in *B*, was measured, and mean fluorescence intensities for all cells (in a.u.) are presented as *scatter plots*. The *horizontal midline* in each plot represents the mean fluorescence intensity, and the *error bars* represent ±S.D. In *D*, the cellular fluorescence was quantified at both 15 and 30 min post-MG-B-TAU addition. Kruskal–Wallis statistical analyses with Dunn's post hoc test were performed, and the statistical significance is indicated (**, $p < 0.001$; ***, $p < 0.0001$; *ns*, $p > 0.01$, not significant). *E*, confocal microscope images of cells expressing FAP-TM-Kir2.1 that were incubated for 90 min with LatA or DMSO and stained with MG-B-TAU for 30 min are shown. *F*, the total cellular fluorescence for $n > 60$ cells, imaged as in *E*, was measured, and mean fluorescence intensities for all cells (in a.u.) are presented as *scatter plots*. A Student's *t* test was performed to assess significance (***, $p < 0.0001$).

ipated, Sec61-FAP– or Sec63-FAP–containing cells incubated with the MG-ESTER dye showed a localization pattern consistent with ER residence, with clear perinuclear and cortical ER rings (40). In contrast, FAP-TM-Kir2.1 incubated with MG-ESTER had a punctate distribution with cortical patches and a region of intracellular exclusion consistent with the nucleus (*Fig. 3B*, *top row*). Under these conditions, it was impossible to discern plasma membrane–localized FAP-TM-Kir2.1 from ER-localized FAP-TM-Kir2.1 using the cell-permeant dye. However, when the same concentration of MG-B-TAU was added for 30 min and images were acquired using identical parameters, a fluorescent signal was absent in the Sec63-FAP–containing cells, yet dim fluorescence was evident for FAP-TM-Kir2.1 (Fig. 3*B*, *second* and *third rows*). This putative plasma membrane pool of FAP-TM-Kir2.1 was enhanced when images were adjusted using post-acquisition modifications (Fig. 3*B*, *third row*). Although the intensity of the cell-surface pool was modest, clear puncta at the cell periphery corresponding to FAP-TM-Kir2.1 were reproducibly observed, whereas no signal was detected for Sec63-FAP (Fig. 3*B*, *bottom row*). When the fluorescent signals for FAP-TM-Kir2.1, Sec61-FAP, and Sec63-FAP were quantified, the signals with the permeant dye were stronger compared with the signals with the impermeant dye (Fig. 3, *C* and *D*). In addition, although the fluorescent signals with the impermeant dye for both FAP-TM-Kir2.1 and Sec63-FAP increased with longer incubation times, suggesting that some cell-impermeant dye may enter the cells over time via bulk endocytosis, the fluorescent signal for FAP-TM-Kir2.1 was significantly brighter than that of the Sec63-FAP control (Fig. 3*D*). Importantly, the signal intensity of FAP-TM-Kir2.1 was ~10-fold higher when it was detected with the permeant *versus* the impermeant dyes (Fig. 3, *C* and *D*). These results are consistent with the biochemical fractionation data indicating that only ~10% of Kir2.1 is found at the cell surface (Fig. 1, *C* and *D*).

Next, we set out to establish that the punctae at the cell periphery represent the plasma membrane pool of FAP-TM-Kir2.1. Specifically, we found that the MG-B-TAU– dependent fluorescence signal rose significantly when the cells were pretreated with latrunculin A (LatA) (Fig. 3, *E* and *F*). LatA blocks actin polymerization and thereby prevents endocytosis, yet it leaves intracellular sorting intact (41). Thus, treatment with LatA allowed FAP-TM-Kir2.1 to accumulate at the cell surface, increasing the FAP-TM-Kir2.1 pool that can be stained with the impermeant dye. Together, these data demonstrate that the MG-B-TAU dye is cell-impermeant in yeast, consistent with what has been reported for MG-B-TAU in mammalian cells (38). Further, when used with a FAP-tagged Kir2.1 chimera, the cell-surface population of this protein can be quantified.

The localization and relative cellular distribution of FAP-TM-Kir2.1 appeared consistent with what we observed previously when the residence of HA-tagged Kir2.1 was queried using indirect immunofluorescence microscopy (Figs. 1*C* and 3, *B–D*) (3). Nevertheless, we wanted to assess the function, stability, and regulation of this new FAP-TM–tagged construct. As evident with the WT and HA-tagged proteins, we found that FAP-TM-Kir2.1 improved growth on low-potassium medium compared with the vector control; however, FAP-TM-Kir2.1 rescued growth less effectively compared with the HA-tagged protein (Fig. 4*A*). Indeed, immunoblot analyses of whole-cell extracts revealed that the steady-state levels of the FAP-TM-Kir2.1 protein were dramatically lower than Kir2.1 (Fig. 4*B*). The reduction in FAP-TM-Kir2.1 was unlikely to arise from altered gene expression because FAP-TM-Kir2.1 and Kir2.1 are expressed from the same promoter. Instead, when the degradation rate of FAP-TM-Kir2.1 was compared with HA-tagged

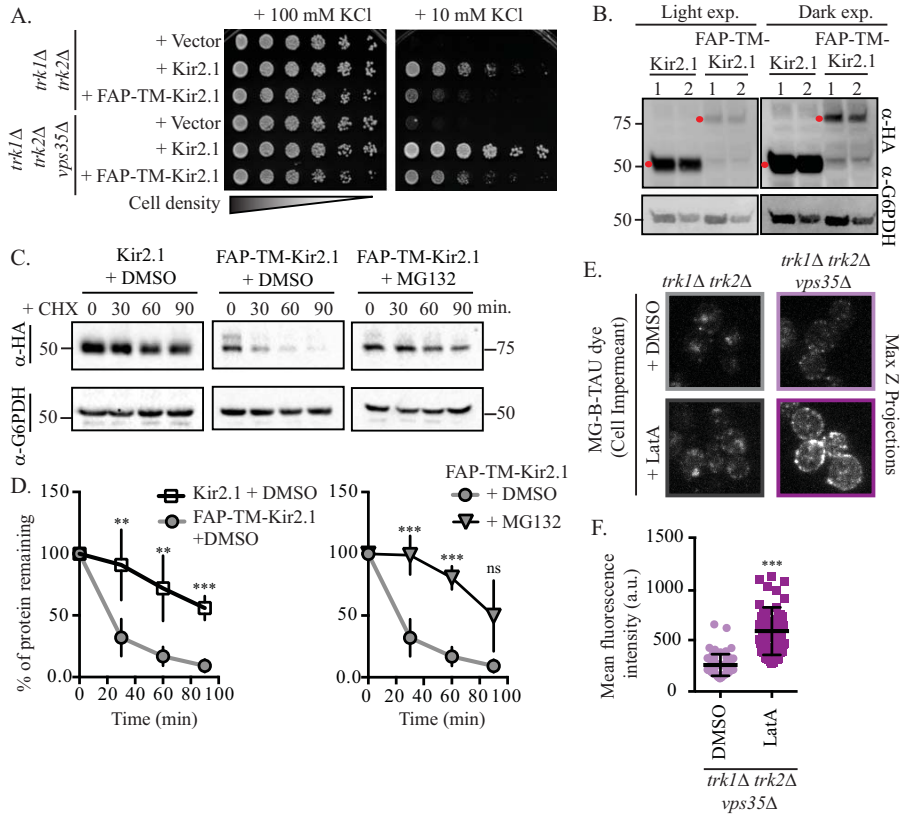

Figure 4. The plasma membrane residence and activity of Kir2.1 and FAP-tagged Kir2.1 are regulated similarly. *A*, growth of serial dilutions of *trk1*Δ *trk2*Δ or *trk1*Δ *trk2*Δ *vps35*Δ cells containing the indicated plasmids on SC medium lacking leucine and containing the indicated amount of KCl is shown. Growth shown is at 4 days. *B*, whole-cell extracts from *trk1*Δ *trk2*Δ cells expressing Kir2.1 or FAP-TM-Kir2.1 were analyzed by immunoblotting. *Red dots* indicate bands of the correct molecular mass for Kir2.1 and FAP-TM-Kir2.1 (α-HA). Molecular masses are denoted in kilodaltons. Whole-cell extracts were loaded at two different concentrations (*lanes* 1 and 2) as shown in the loading control (α-G6PDH). Two different exposures of the same blot are shown to facilitate comparisons. *C*, yeast cells (*trk1*Δ *trk2*Δ *pdr5*Δ) expressing either HA-tagged or FAP-tagged Kir2.1 were grown to mid-logarithmic phase, treated with either MG132 or DMSO (vehicle control), and dosed with cycloheximide (*CHX*), and samples were taken at the indicated time points. Kir2.1 protein abundance was assessed by immunoblotting with the indicated antibodies. Molecular masses are denoted in kilodaltons. *D*, immunoblots as in *C* were quantified for a minimum of four replicate experiments, and the means are plotted. Data are normalized to 100% for $t = 0$ time point in each case. *Error bars* represent ±S.D., and a Student's *t* test was performed to assess significance (**, $p < 0.001$; ***, $p < 0.0001$; *ns* = $p > 0.01$, not significant). *E*, *trk1*Δ *trk2*Δ or *trk1*Δ *trk2*Δ *vps35*Δ cells expressing FAP-TM-Kir2.1 were treated with LatA or DMSO for 90 min and then incubated with MG-B-TAU dye for 30 min and imaged by confocal microscopy. *F*, total cellular fluorescence for $n > 50$ cells, imaged as in *C*, was measured, and mean fluorescence intensities for all cells (in a.u.) is presented as *scatter plots*. A Student's *t* test was performed to assess significance (***, $p < 0.0001$).

Kir2.1, we found that FAP-tagged Kir2.1 was significantly less stable that the HA-tagged Kir2.1 (Fig. 4, *C* and *D*). Inhibition of the proteasome via incubation of cells with MG132 significantly stabilized FAP-tagged Kir2.1 (Fig. 4, *C* and *D*), demonstrating that the FAP-tagged Kir2.1 is subject to proteasome-mediated degradation. Next, to determine whether the degradation of FAP-TM-Kir2.1 was regulated by the same factors acting in the late secretory pathway as reported previously for Kir2.1 (3), we examined FAP-TM-Kir2.1 activity and localization in cells lacking the retromer subunit Vps35. Consistent with our previous findings, Kir2.1-dependent growth on low-potassium medium was greatly enhanced in a *vps35*Δ *trk1*Δ *trk2*Δ strain compared with *trk1*Δ *trk2*Δ cells, and growth rescue mediated by FAP-TM-Kir2.1 in this strain background was similarly improved on low-potassium medium (Fig. 4*A*). Moreover, we found that FAP-TM-Kir2.1 levels at the cell surface, as assessed with MG-B-TAU, increased in cells lacking Vps35 (Fig. 4, *E* and *F*). Although the protein is less stable than HA-Kir2.1, these combined data indicate that FAP-TM-Kir2.1 is a functional potassium channel whose trafficking itinerary is consistent with that of the active HA-tagged protein (3).

α-Arrestins increase Kir2.1 residence at the plasma membrane in a Rsp5-dependent manner

Based on the data presented in Fig. 1, α-arrestin overexpression should augment cell-surface residence of Kir2.1 at the plasma membrane. Therefore, we employed the FAP-TM-Kir2.1 chimera to determine whether increased staining with MG-B-TAU dye was apparent when the α-arrestins were overexpressed. As hypothesized, cells overexpressing α-arrestins Aly1, Aly2, or Ldb19 had significantly brighter FAP-TM-Kir2.1–dependent cell-surface fluorescence compared with cells with a vector control (Fig. 5, *A* and *B*). To ensure that increased fluorescence intensity was not caused by a reduced rate of endocytosis, but rather corresponded to an elevated rate of delivery to the plasma membrane, we pretreated cells with LatA and then added MG-B-TAU before conducting image analysis by confocal microscopy. At the concentrations used (200 μM), LatA resulted in loss of both filamentous actin and cortical actin patches, the latter of which is associated with yeast endocytosis. Consequently, this concentration completely prevents fluid phase endocytosis of lucifer yellow (41–

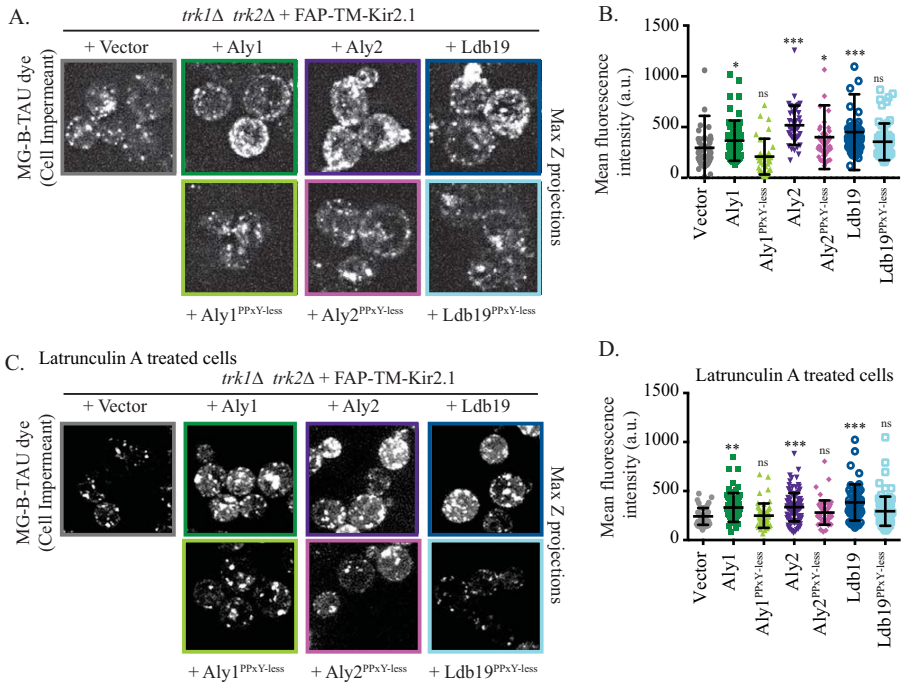

Figure 5. α-Arrestin regulation of Kir2.1 requires the Rsp5 ubiquitin ligase. *A*, maximum Z-projections of confocal microscopy images were acquired in *trk1*Δ *trk2*Δ cells expressing FAP-TM-Kir2.1 and in the presence of a vector control or plasmids overexpressing the indicated α-arrestins. The cells were incubation with MG-B-TAU dye for 30 min. *B*, total cellular fluorescence for the maximum Z-projections of $n > 30$ cells, imaged as in *A*, was measured, and mean fluorescence intensities for all cells (in a.u.) are presented as *scatter plots*. The *horizontal midline* in each plot represents the mean fluorescence intensity, and the *error bars* represent ±S.D. Kruskal–Wallis statistical analyses with Dunn's post hoc test were performed, and the statistical significance compared with the vector control is indicated (*p* values are assigned as listed below). *C*, maximum Z-projections of confocal microscopy images were acquired in *trk1*Δ *trk2*Δ cells expressing FAP-TM-Kir2.1 and containing the vector control or plasmids overexpressing the indicated α-arrestins. The cells were incubation with LatA for 90 min and the MG-B-TAU dye for 30 min. *D*, total cellular fluorescence for the maximum Z-projections of $n > 50$ cells, imaged as in *C*, was measured, and mean fluorescence intensities for all cells (in a.u.) are presented as *scatter plots*. The *horizontal midline* in each plot represents the mean fluorescence intensity, and the *error bars* represent ±S.D. Kruskal–Wallis statistical analyses with Dunn's post hoc test were performed (*, $p < 0.01$; **, $p < 0.001$; ***, $p < 0.0001$; *ns*, $p > 0.01$, not significant).

43). Thus, in our experiments, endocytosis was completely blocked but delivery to the cell surface remained intact. As shown in Fig. 5, *C* and *D*, greater FAP-TM-Kir2.1 cell-surface fluorescence was detected when *ALY1*, *ALY2*, or *LDB19* was overexpressed compared with the vector control in the LatA-treated cells. These data demonstrate that the α-arrestins facilitate Kir2.1 delivery to the cell surface and do not require Kir2.1 endocytosis to impact Kir2.1 abundance at the cell surface.

All α-arrestins in yeast contain (L/P)P*X*Y motifs. This motif binds WW-domains in a ubiquitin ligase, Rsp5, which is involved in the trafficking of several α-arrestin–dependent cargo proteins (19, 20, 31, 44, 45). However, exceptions have been noted in which Rsp5 function during the sorting of α-arrestin–dependent cargo proteins was dispensable (17). We previously showed that Aly1, Aly2, and Ldb19 mutants where each of the (L/P)P*X*Y motifs is altered to (L/P)P*X*G (referred to hereafter as Aly1^{PP}*X*Y-less, Aly2^{PP}*X*Y-less, and Ldb19^{PP}*X*Y-less) were unable to bind Rsp5. These PP*X*Y-less mutants of Aly1, Aly2, and Ldb19 also failed to regulate clathrin-mediated or clathrin-independent endocytosis of the G protein–coupled receptors Ste2 and Ste3 (17, 46). To investigate the role of the Rsp5-binding motif in Kir2.1 trafficking, we examined the PP*X*Y-less mutants of Aly1 and Aly2 and found that sensitivity to azetidine-2-carboxylic acid (AzC) is lost, a phenotype associated with a defect in Gap1 sorting to the plasma membrane (Fig. S2*C*) (22, 30). Consistent with these data, even though overexpression of Aly1, Aly2, or Ldb19 promoted Kir2.1-dependent growth on low-potassium medium (Figs. 1*A* and 6*A*), the PP*X*Y-less mutant forms of these α-arrestins were dramatically less effective than their WT counterparts (Fig. 6*A*). It should be noted that overexpression of any of these α-arrestins, either the PP*X*Y-less mutants or their WT counterparts, did not significantly alter the steady-state abundance of Kir2.1 compared with the vector control. This result was evident regardless of whether the *TEF1pr*-Kir2.1 expression system or the *ZWF1pr*-Kir2.1 expression system was used (data not shown and Fig. S1*C*). Consistent with an important role for Rsp5 in regulating Kir2.1 activity at the cell surface, there was less Kir2.1 at the cell surface in each of the α-arrestin PP*X*Y-less mutants than in cells expressing their WT counterpart (Fig. 5). In almost all cases, the PP*X*Y-less mutants did not significantly increase cell-surface Kir2.1 abundance compared with the vector control; only a modest increase in cell-surface abundance was uncovered with Aly2^{PP}*X*Y-less. Further evidence supporting Rsp5-dependent trafficking was apparent because PP*X*Y-less α-arrestins failed to elevate intracellular potassium compared with the vector control when assessed by ICP-MS. In contrast, the WT Aly1, Aly2, and Ldb19 α-arrestins significantly increased intracellular potassium (Fig. 6*B*). These data strongly suggest that the binding of select α-arrestins to Rsp5 promotes Kir2.1 trafficking to the cell surface.

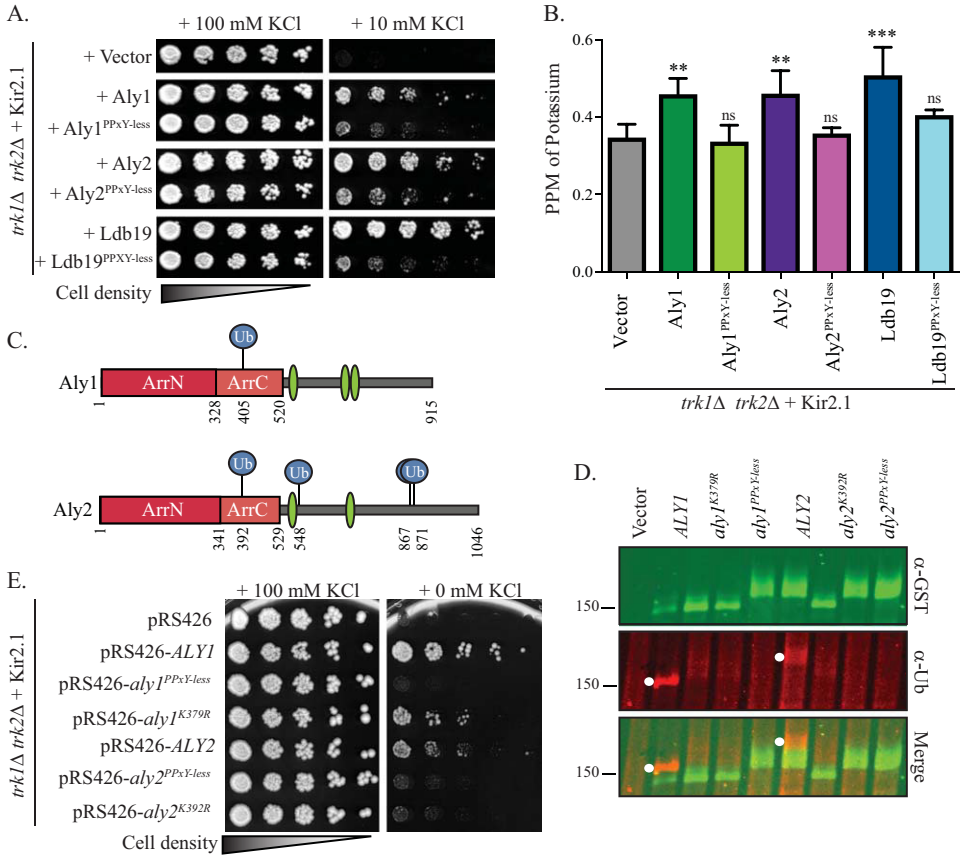

Figure 6. Overexpression of Aly1, Aly2, and Ldb19 increases both Kir2.1 residence at the plasma membrane and intracellular potassium. *A*, growth of serial dilutions of *trk1*Δ *trk2*Δ cells containing the indicated plasmids on SC medium lacking leucine and uracil and containing the indicated added amounts of KCl is shown after 2 days. *B*, *trk1*Δ *trk2*Δ cells expressing Kir2.1 and the indicated overexpressed α-arrestin plasmids were grown in 10 mM KCl, and cellular potassium levels were measured using ICP-MS. The ppm corresponding to KCl for an equivalent number of cells was determined for four replicates, and the mean ± S.D. was calculated (presented as *error bars*). Kruskal–Wallis statistical analyses with Dunn's post hoc test were performed, and the statistical significance compared with the vector control for each is indicated (**, $p < 0.001$; ***, $p < 0.0001$; *ns*, $p > 0.01$, not significant). *C*, schematic of the Aly1 and Aly2 protein coding regions, where the *numbers* indicate the amino acid position, *dark red boxes* denote the N-terminal arrestin-fold, the *light red boxes* denote the C-terminal arrestin-fold, *green ovals* indicate the position of the (L/P)PXY motifs, and *blue circles* indicate the sites of ubiquitin (*Ub*) modification identified via MS. *D*, GST-fused α-arrestins were isolated from WT (BJ5459) cells after α-arrestin expression (under control of the *CUP1* promoter) was induced with copper sulfate. Isolated proteins were resolved by SDS-PAGE and immunoblotted with the indicated antibodies. Molecular masses are denoted in kilodaltons. *E*, growth of serial dilutions of *trk1*Δ *trk2*Δ cells containing the indicated plasmids on SC medium lacking leucine and uracil and containing the indicated added amounts of KCl is shown after 4 days.

One hypothesis for why Rsp5 is needed to increase Kir2.1 abundance at the cell surface is that Rsp5 ubiquitination of the α-arrestins is required for their role in intracellular protein sorting. For many α-arrestins, monoubiquitination is linked to the regulation of protein trafficking, and loss of monoubiquitination impairs α-arrestin recruitment to membranes and interactions with key trafficking factors (18, 19, 47). To test this hypothesis for Aly1 and Aly2, we performed LC-MS analysis of isolated GST-tagged Aly1 and Aly2 from WT yeast. Spectra corresponding to peptides covering 60 and 56% of Aly1 and Aly2, respectively, were obtained (Fig. S2, *B* and *C*), and diglycine-modified lysines, a signature of ubiquitination in MS spectra (48–50), were identified at the positions indicated (Figs. 6*C* and S2, *A* and *B*). Notably, modification of Lys-392 in Aly2 was identified in our analyses and also in three other proteomics studies (51–53), lending strong support for this position as a valid ubiquitination site. We mapped the ubiquitination sites onto the Phyre-predicted secondary structures of Aly1 and Aly2 (Fig. 6*C*) (30, 54, 55) and found that Lys-392 in Aly2 corresponds to the conserved Lys-379 site in Aly1, which also had been identified as being ubiquitinated in a proteomic screen (52). In addition, based on secondary structure predictions, the Lys-392 and Lys-379 sites in Aly1 and Aly2, respectively, map to the same region within the C-terminal arrestin-fold as one of the four monoubiquitination sites in Rod1 (data not shown and Ref. 18). Based on these observations, we mutated Lys-392 in Aly2 and the analogous Lys-379 residue in Aly1 to arginine using site-directed mutagenesis and examined the ubiquitination status of the resulting mutant α-arrestins via immunoblot analysis. Although ubiquitination was clearly detected for the WT Aly1 and Aly2 species, Aly1^{K379R} and Aly2^{K392R} lacked a discernible ubiquitin signal (Fig. 6*D*). As a control in these experiments, Aly1$^{PY\text{-}less}$ and Aly2$^{PY\text{-}less}$ were also employed, and a similar loss of ubiquitination (Fig. 6*D*), as anticipated based on previous findings (22), was observed. These results confirmed that select lysines are ubiquitinated in Aly1 and Aly2.

We then assessed the impact of the Lys-to-Arg mutations in Aly1 and Aly2 on known phenotypes associated with overexpression of WT Aly1 and Aly2, such as resistance to rapamycin

and sensitivity to AzC (see above and Refs. 22 and 30). We found that loss of these ubiquitination sites resulted in hypomorphic Aly1 and Aly2 alleles that were less effective at conferring sensitivity to AzC, suggesting a reduced ability to promote Gap1 trafficking to the plasma membrane (Fig. S2*C*). Although ubiquitination was dispensable for Aly1-induced resistance to rapamycin, the modification was required for Aly2-induced resistance to rapamycin (Fig. S2*C*). These data suggest that ubiquitination at these sites is important for some but not all Aly1- or Aly2-mediated activities. Finally, we examined the ability of the ubiquitination-deficient Aly1 and Aly2 mutants to promote Kir2.1 activity by monitoring their ability to promote growth on low-potassium medium. Interestingly, both *ALY1*^{K392R} and *ALY2*^{K379R} were hypomorphic to their respective WT alleles (Fig. 6*E*), showing a reduced capacity for growth on low-potassium medium. As observed above, the PP*XY*-less mutants were also unable to stimulate Kir2.1-depenent growth on low potassium. Taken together, these findings suggest that ubiquitination of Aly1 and Aly2 is essential for optimal Kir2.1 trafficking to the cell surface. In addition, binding of Aly1, Aly2, and Ldb19 to the Rsp5 ubiquitin ligase also appears to be required for α-arrestin–dependent delivery of Kir2.1 to the plasma membrane.

α-Arrestin phosphorylation impacts Kir2.1 trafficking

α-Arrestins are heavily phosphorylated. Thus far, more than 24 and 13 phosphorylated residues have been identified in Aly1 and Ldb19, respectively, using MS (22, 52, 56–58). In many, but not all instances, phosphorylated α-arrestins fail to stimulate endocytosis of the associated membrane proteins, whereas dephosphorylated α-arrestins are more potent regulators of endocytosis (18, 22, 58–60). Previously, we found that Aly1 is dephosphorylated by the protein phosphatase calcineurin (22) and that dephosphorylation stimulates Aly1-mediated endocytosis of the aspartic acid permease Dip5. However, the calcineurin-mediated dephosphorylation of Aly1 had no effect on Aly1-dependent recycling of the Gap1 permease (22). These data indicate that the action of calcineurin on a given α-arrestin can affect the trafficking of specific cargo proteins. Therefore, to uncover the potential role of α-arrestin phosphorylation on Kir2.1 trafficking, we mutated the calcineurin-binding site in Aly1, PILKIN (aa 832–837), to a series of alanines (*ALY1*^{AAAAAA}) (22), and the protein was overexpressed. In this strain, Kir2.1-dependent growth on low potassium was enhanced (Fig. 7*A*). Consistent with these data, intracellular potassium as well as FAP-TM-Kir2.1 residence at the cell surface was also enhanced when the Aly1^{AAAAAA} protein was overexpressed (Fig. 7, *B–D*).

To further assess the role of calcineurin in regulating Aly1, we deleted the gene encoding the calcineurin regulatory subunit *CNB1*, which is required for catalytic activity (61), in the *trk1*Δ *trk2*Δ strain background. We then measured the ability of Aly1 to promote Kir2.1-dependent growth on low potassium. As shown in Fig. 7*E*, we found that the absence of calcineurin activity augmented Aly1-mediated growth on low-potassium medium, consistent with the phosphorylated form favoring Kir2.1 residence at the cell surface. Based on these combined data, we propose a model whereby calcineurin-mediated dephosphorylation of Aly1 impairs the ability of an α-arrestin to stimulate Kir2.1 trafficking to the cell surface (Fig. 7*F*). We further propose that phosphorylation serves as a molecular switch: dephosphorylated Aly1 stimulates endocytosis, whereas phosphorylated Aly1 recognizes the intracellular pool of select integral membrane proteins and stimulates their trafficking to the cell surface (Fig. 7*F*).

Discussion

By applying a genetic analysis in a yeast model, we demonstrated that select α-arrestins regulate Kir2.1 cell-surface abundance by facilitating channel trafficking to the plasma membrane. Confirmation that the α-arrestins directly affect Kir2.1 function at the plasma membrane, and consequently an increase in intracellular potassium, was uncovered by applying a spectroscopic technique that is rarely used in yeast, ICP-MS. Our results confirm the general applicability of this method for future studies on the function of any plasma membrane resident ion channel in this organism. Consistent with previous studies, we also found that the α-arrestin–mediated effect on Kir2.1 requires α-arrestin phosphorylation and interaction with a ubiquitin ligase, Rsp5, that plays an important role in regulating the trafficking of myriad transporters and other plasma membrane cargo (18–20, 22, 31, 44, 58, 59). In addition, for the first time we also applied the FAP-tagging system to demonstrate that this technique can differentiate a cell surface–localized protein pool from the intracellular pool in yeast. Consequently, this technology may now become widely applicable in protein trafficking studies in this organism, which thus far have relied on cell-surface biotinylation, which is of low efficiency and may permeabilize cells (62), or on GFP-tagging methods, which may not easily quantify or differentiate between intracellular *versus* cell-surface protein pools (63, 64). We envision that the FAP system will next allow for fine spatial and temporal endocytic dynamics to be resolved for any endogenous yeast protein without interference from the competing intracellular fluorescence signal, which is inherent in this organism (63–65).

As opposed to the well-document role of α-arrestins in regulating endocytosis (18–21, 31, 44), we have shown that Aly1, Aly2, and Ldb19 promote Kir2.1 localization to the cell surface. However, distinct from their function during endocytosis, the role of α-arrestins in regulating the intracellular recycling pathways is still emerging. Indeed, our discovery that α-arrestins augment Kir2.1 cell-surface abundance is reminiscent of a related activity observed for Aly1 and Aly2 in increasing the abundance of the general amino acid permease Gap1 at the cell surface after nutrient deprivation (30). Aly2-dependent recycling of Gap1 requires both phosphoregulation of Aly2 by the Npr1 kinase, which is negatively regulated by TORC1 and has long been known to be a positive regulator of Gap1 trafficking to the cell surface (30, 35, 58, 66, 67), and also AP-1, the clathrin adaptor essential for endosome-to-Golgi retrieval of select cargo proteins (68–70). Our current model for Aly2-mediated recycling of Gap1 is that Aly2 stimulates Gap1 packaging into AP-1 and clathrin-coated vesicles that shuttle Gap1 from endosomes to the trans-Golgi network. Aly2 is a substrate for Npr1 *in vitro*, and Npr1is required for Aly2-dependent regulation of

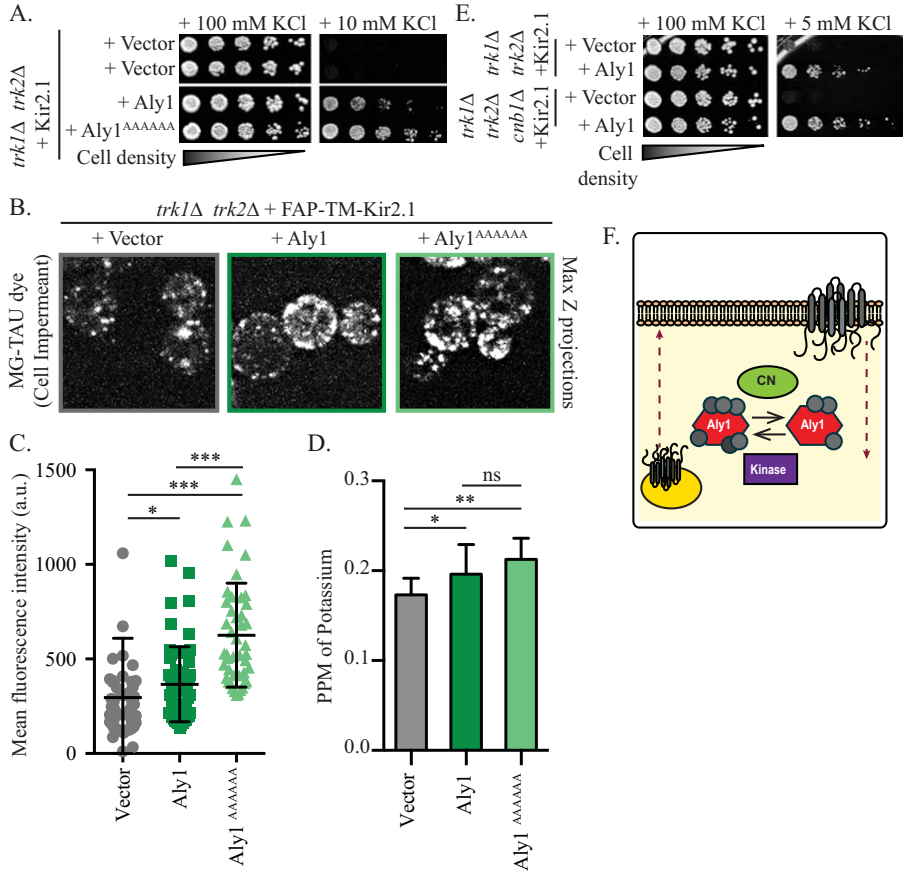

Figure 7. Calcineurin negatively regulates Aly1-mediated Kir2.1 trafficking to the plasma membrane. *A*, growth of serial dilutions of *trk1*Δ *trk2*Δ cells containing the indicated plasmids on SC medium lacking leucine and uracil and containing the indicated amount of KCl is shown after 2 days. *B*, maximum Z-projections (*Max Z*) of confocal microscopy images acquired in *trk1*Δ *trk2*Δ cells expressing FAP-TM-Kir2.1 and containing a vector control or plasmids overexpressing the indicated α-arrestins. Cells were incubated with MG-B-TAU dye for 30 min. *C*, total cellular fluorescence for the maximum Z-projections of $n > 45$ cells, imaged as in *B*, was measured, and mean fluorescence intensities for all cells (in a.u.) are presented as *scatter plots*. The *horizontal midline* in each plot represents the mean fluorescence intensity, and the *error bars* represent ±S.D. Kruskal–Wallis statistical analyses with Dunn's post hoc test were performed, and the statistical significance compared with the vector control is indicated. *D*, *trk1*Δ *trk2*Δ cells expressing Kir2.1 and the indicated overexpression α-arrestin plasmids were grown in 10 mM KCl and cellular potassium levels were measured by ICP-MS. The PPM of KCl for an equivalent number of cells was determined for 4 replicates, and the mean and S.D. were calculated (presented as error bars). Kruskal–Wallis statistical analyses with Dunn's post hoc test were performed, and the statistical significance compared with the vector control for each is indicated (*, $p < 0.01$; **, $p < 0.001$; ***, $p < 0.0001$; *ns*, $p > 0.01$, not significant). *E*, growth of serial dilutions of *trk1*Δ *trk2*Δ or *trk1*Δ *trk2*Δ *cnb1*Δ cells containing the indicated plasmids on SC medium lacking leucine and uracil and containing the indicated amount of KCl is shown after 2 days. *F*, model for calcineurin (*CN*) regulation of Aly1-mediated trafficking of Kir2.1 *Red dashed lines* indicate exocytosis or endocytosis of Kir2.1. *Gray circles* on Aly1 indicate phosphorylation sites, with fewer phosphorylation sites in the version of Aly1 that has been dephosphorylated by calcineurin.

Gap1 trafficking, making it likely that Npr1 phosphorylation of Aly2 *in vivo* stimulates Aly2-mediated Gap1 recycling (30). Therefore, we propose that Aly2 operates similarly to increase Kir2.1 cell-surface localization by enhancing endosome-to-Golgi trafficking of Kir2.1, ultimately increasing Kir2.1 localization at the plasma membrane.

We also describe here a novel role for calcineurin-associated Aly1 dephosphorylation as an inhibitory signal during Kir2.1 trafficking to the cell surface. This result suggests that phosphorylation/dephosphorylation of Aly1 may serve as a functional switch in which dephosphorylated Aly1 stimulates cargo endocytosis (as seen for another cargo, Dip5 (22, 44)), whereas phosphorylated Aly1 promotes anterograde cargo trafficking (as seen for Kir2.1 in this study). Future studies will delineate the intracellular sorting pathway(s) controlled by Aly1 via this switch and establish whether a conformational change in Aly1 triggers these distinct responses. Interestingly, the calcineurin-mediated negative regulation of Kir2.1, as shown here, may be conserved in more complex organisms (71–73). For example, in mammalian cells, Kir2.1 interacts with the protein kinase A–anchoring protein (AKAP), which scaffolds multiple kinases and phosphatases (including calcineurin). Association with AKAP increases Kir2.1 channel function when calcineurin and other phosphatases are inhibited. Consequently, Kir2.1 may be negatively regulated in a similar fashion by calcineurin in higher organisms (72). In addition, pharmacological inhibition of calcineurin decreases Kir2.1 channel activity at the cell surface in *Xenopus* oocytes (71), and calcium influx as an indirect result of Kir2.1 hyperpolarization activates calcineurin to stimulate myocyte development (73).

In contrast to Aly1 and Aly2 (30), Ldb19-mediated protein recycling has not been described previously, and thus our findings add a new dimension to the functional repertoire for this α-arrestin. Nevertheless, Aly1, Aly2, and Ldb19 have overlapping functions in regulating the clathrin-independent and clathrin-mediated endocytosis of the yeast mating pheromone

receptor Ste3 (46). In support of a broader role for α-arrestins in regulating intracellular sorting, another α-arrestin, Rod1, controls a complex intracellular trafficking itinerary for the lactate permease Jen1. In this case, Rod1 regulates the glucose-induced, Rsp5-dependent endocytosis of Jen1, but after internalization Jen1 traffics from endosomes to the Golgi rather than being routed from endosomes to the vacuole for degradation (29). Subsequently, Rod1 is recruited to Golgi membranes and facilitates Jen1 retrieval and return to endosomes, which subsequently induces Jen1 trafficking to and degradation in the vacuole. The role of Rod1 in regulating this two-step protein "shuffle" demonstrates both the functional plasticity of α-arrestin–mediated trafficking and the complex itinerary of intracellular trafficking. In fact, a similar role has been described for two other α-arrestins, Bul1 and Bul2, which stimulate Gap1 endocytosis as well as Golgi-to-endosome sorting (32, 36, 60, 74). A more detailed definition of the mechanism by which Aly1, Aly2, and Ldb19 regulate Kir2.1 trafficking in yeast and mammalian cells represents an important area of study and is in progress. However, it should be noted that it is not trivial to definitively link a given α-arrestin in yeast with a homolog or even a paralog in human cells, as members of the α-arrestin family are defined by a structural motif as well as by their functional association with ubiquitin ligases and cargo proteins (33, 75). Yet, the amino acid sequence conservation between α-arrestins within a given organism and even more so between different organisms is exceeding low (33, 75).

Our earlier study defined a role for the ESCRT machinery, retromer, and AP-1, as well as other Rsp5 adaptor proteins (*e.g.* Bsd2 and Tre1) in regulating Kir2.1 activity at the cell surface (3). For example, loss of an ESCRT-1 component, Vps23, improves yeast growth on low-potassium medium, consistent with Kir2.1 trafficking into the MVB pathway and on to the vacuole for degradation (3). The regulation of Kir2.1 by ESCRT is conserved, as both the knockdown of ESCRT components or pharmacological inhibition of lysosomal degradation increases Kir2.1 abundance in HEK293 cells. Consistent with Kir2.1 trafficking to the MVB pathway in yeast, the loss of Bsd2 or Tre1, which represent other Rsp5 adaptors that stimulate cargo ubiquitination and trafficking to the vacuole (76, 77), augments growth of Kir2.1-expressing yeast on low-potassium medium (3). Thus, Bsd2 and Tre1 may help direct Rsp5 ubiquitination onto Kir2.1 to promote vacuolar trafficking, whereas the α-arrestins act instead as trafficking adaptors to stimulate the recycling of Kir2.1 from endosomes back to the Golgi or directly to the cell surface. It is interesting that loss-of-function mutations in any one of four other factors important for endosome-to-Golgi sorting (retromer, GARP, AP-1, and Ypt6) were also identified in our yeast screen. We posit that the loss of these endosome-to-Golgi recycling components impairs the MVB-dependent sorting of Kir2.1, based on the model described above for Jen1 regulation by an α-arrestin (29). Alternatively, loss of these endosome-to-Golgi sorting factors may lead to compensatory changes in protein trafficking that either allow for direct transit of Kir2.1 from endosomes to the cell surface or improve the activity of other intracellular recycling pathways. Defining how these intracellular sorting pathways contribute to α-arrestin–mediated trafficking will also be a topic for future efforts.

In addition to defining a role for α-arrestins in stimulating Kir2.1 trafficking to the cell surface and demonstrating that Aly1 dephosphorylation negatively regulates this pathway, our results strongly suggest that the α-arrestins bind Rsp5 to enhance Kir2.1 cell-surface localization. One of the hallmarks of α-arrestins is that they contain (L/P)P*X*Y motifs and thus bind WW domains in the Rsp5 ubiquitin ligase, whose ortholog in mammals is Nedd4-2 (19–21, 33, 45, 78). During endocytosis, α-arrestins bridge plasma membrane cargo proteins and Rsp5 (18–21). Rsp5 can then ubiquitinate the cargo proteins, which triggers endocytosis but also ubiquitinates the α-arrestin (18, 19, 31). In some instances, α-arrestin lysine mutants, which cannot be ubiquitinated, are nonfunctional (17–19, 31), and it has been suggested that monoubiquitination is needed to activate an α-arrestin during protein trafficking (79). For example, monoubiquitination of Rod1 is required to regulate Jen1 trafficking (18), and similarly, monoubiquitination of Ldb19 is critical for Can1 trafficking (19). Interestingly, the loss of Ldb19 monoubiquitination impairs the recruitment of this α-arrestin to the Golgi and plasma membranes (19), suggesting that monoubiquitination may play an important role during intracellular sorting as well as endocytosis. Loss of α-arrestin Rim8 monoubiquitination reduces binding to the ESCRT subunit Vps23 and diminishes Rim8 function (80), suggesting that monoubiquitination can influence α-arrestin binding to key protein-trafficking regulators. In this study, we identified the site of Aly1 and Aly2 monoubiquitination and showed that mutant forms of Aly1 and Aly2, which cannot be modified, are unable to effectively promote Kir2.1-dependent growth on low potassium. Thus, as is the case for many other α-arrestins, monoubiquitination of Aly1 and Aly2 facilitates the trafficking of distinct cargo proteins. Based on these data, we propose that our PPXY-less Aly1, Aly2, and Ldb19 mutants may exhibit compromised function, not because of their inability to recruit Rsp5 to Kir2.1 but perhaps as a result of their inability to be recruited to membranes or bind auxiliary factors that promote intracellular Kir2.1 sorting. Here, too, future in-depth studies will be needed to establish whether this principle applies to the sorting of Kir2.1 in yeast and mammalian cells.

Experimental procedures

Yeast strains and growth conditions

Yeast strains used in this study and their construction are described in Table 1. Yeast were grown in synthetic complete (SC) medium prepared as described (81). SC low-potassium medium was also prepared as described with the use of monosodium glutamate as a nitrogen source, the addition of 20 mM MES to maintain the pH, and the indicated amount of KCl (3). Liquid medium was filter-sterilized, and for plated medium, 2% (w/v) agar was added prior to autoclaving. Plasmids were transformed into yeast via the lithium-acetate method and selected for on the appropriate SC medium. Yeast cells were grown at 30 °C unless otherwise indicated. For growth assays on solid medium, 5-fold serial dilutions of saturated, overnight cultures

Table 1
Yeast strains used in this study

Strain	Genotype	Source
BY4741	*MATa his3Δ1 leu2Δ0 ura3Δ0 met15Δ0*	(89)
BY4743	*MATa/MATa his3Δ1/his3Δ1 leu2Δ0/ leu2Δ0 ura3Δ0/ura3Δ0 met15Δ0/MET15 LYS2/lys2Δ0*	(89)
trk1Δtrk2Δ	*MATα trk1Δ::HIS3 trk2Δ::HIS3 his3Δ200 leu2Δ1 ura3–52 trp1–1 ade2*	(16, 90)
Query strain *trk1Δtrk2Δ* (YAK01)	*MATα trk1Δ::URA3 trk2Δ::NAT his3Δ1 leu2Δ0 ura3Δ0 lyp1Δ0 lysΔ0 can1Δ::STE2pr-HIS3*	(3)
trk1Δtrk2Δvps35Δ	*MATα trk1Δ::URA3 trk2Δ::NAT vps35Δ::KAN his3Δ1 leu2Δ0 ura3Δ0 lyp1Δ0 lysΔ0 can1Δ::STE2pr-HIS3*	This study. This strain was derived from YAK01. VPS35 coding region was replaced by the KAN cassette as described in Ref. 91.
trk1Δtrk2Δcnb1Δ	*MATα trk1Δ::HIS3 trk2Δ::HIS3 cnb1Δ::HPH his3Δ200 leu2Δ1 ura3–52 trp1–1 ade2*	This study. This strain was derived from the *trk1Δtrk2Δ* strain described in Refs. 16 and 89. The *CNB1* coding region was replaced by the hygromycin resistance cassette as described in 90.
HRD1/DOA10 (WT)	*MATα ade2 his3 leu2 ura3 trp1*	(3, 92)
pdr5Δ	*MATα pdr5Δ::KAN his3Δ1 leu2Δ0 ura3Δ0 lys2Δ0*	(93)
BJ5459	*MATa his3Δ200 leu2Δ1 ura3–52 trp1 lys2–801 pep4Δ::HIS3 prb1Δ1.6R can1 GAL*	(94)

(starting concentration of 1.0×10^7 cells/ml) were plated onto the indicated medium and grown for 3–6 days at 30 °C.

Plasmids and DNA manipulations

Plasmids used in this study and details of their construction are described in Table S1. PCR amplifications were performed using Phusion High Fidelity DNA polymerase (Thermo Fisher Scientific, Waltham, MA), and all constructs generated were verified using Sanger sequencing (Genewiz, South Plainfield, NJ).

Yeast protein extraction and immunoblot analysis

Whole-cell extracts of yeast proteins were made by growing cells in low-potassium SC medium supplemented with the indicated amount of KCl to mid-exponential phase at 30 °C (A_{600} = 0.6–0.8) and harvesting equivalent numbers of cells by centrifugation. Cell pellets were flash-frozen in liquid nitrogen and stored at −80 °C until processing. Cells were then lysed using sodium hydroxide, and proteins were precipitated using trichloroacetic acid (TCA) as described (82). The protein precipitates were solubilized in SDS/urea sample buffer (22) and heated to 37 °C for 15 min. Extracts were resolved by SDS-PAGE, and proteins were identified by immunoblotting with mouse anti-HA antibody (Santa Cruz Biotechnology, Santa Cruz, CA) to detect Kir2.1 and rabbit anti-Zwf1 (glucose-6-phosphate dehydrogenase, referred to as G6PDH) antibody (Sigma) as a protein loading control. Anti-Sec61 antibody (83) and anti-Pma1 (40B7 Abcam, Cambridge, MA) were also used where indicated. Anti-mouse or anti-rabbit secondary antibodies conjugated to IRDye 800 or IRDye 680 (Li-Cor Biosciences, Lincoln, NE) were detected using an Odyssey™ Fc IR imaging system (LI-COR Biosciences), or where indicated, horseradish peroxidase-conjugated anti-rabbit immunoglobulin secondary antibody was applied (Jackson ImmunoResearch, West Grove, PA) and was detected with the Supersignal chemiluminescent substrate (Pierce). In this case, images were processed on a Bio-Rad ChemiDoc XRS+ image station with Image Lab 5.2.1 software (Hercules, CA).

Protein stability assays

Yeast cells lacking *PDR5* and transformed with Kir2.1-HA or FAP-tagged Kir2.1 (expressed under the constitutive *TEF1* promoter) were grown overnight to saturation, inoculated at an A_{600} of 0.25 into low-potassium SC medium supplemented with 100 mM KCl, and allowed to grow to mid-log phase at 30 °C. To inhibit the proteasome, cultures were treated with 100 μM MG132 (Selleck Chemicals, Houston, TX) in DMSO or an equivalent amount of the DMSO vehicle as a control, and incubated with agitation for 30 min at 37 °C. At this point, 150 μg/ml cycloheximide (Sigma) was added to each culture to halt protein translation, and cells were further incubated with agitation at 37 °C. Total 1-ml aliquots were withdrawn at 0, 30, 60, and 90 min after the addition of cycloheximide, 17.5 mM NaN_3 was added, and cells were harvested by centrifugation and flash-frozen in liquid nitrogen. Whole-cell extracts were prepared by the TCA precipitation method described above and analyzed via SDS-PAGE and immunoblotting. Immunoblotting used the same antibodies and chemiluminescent

methodology as described above for horseradish peroxidase-conjugated antibodies.

Biochemical fractionation

The subcellular distribution of Kir2.1 was assessed by sucrose gradient sedimentation assays as described (84). In brief, 40 ml of the indicated yeast cultures were grown to an A_{600} of 0.8, harvested by centrifugation, and lysed by glass-bead agitation as described (3). Clarified cell lysates were layered onto a 30–70% sucrose gradient cushion and centrifuged at 100,000 × *g* in a Beckman SW41 rotor for 14 h at 4 °C. Equal fractions were then collected by pipetting from the top of the tube, and proteins were assessed by SDS-PAGE and immunoblotting. Signal intensity was quantified by obtaining densitometry measurements of bands within the linear range of detection using ImageJ software (National Institutes of Health, Bethesda, MD).

Biochemical purification and MS analyses

GST-fused Aly1 or Aly2 was expressed from pKK212-derived plasmids under the control of the *CUP1* promoter in BJ5459 cells as described (22). In brief, cells were grown to mid-exponential phase, and expression was induced from the *CUP1* promoter by the addition of 200 μm CuSO4 for 1 h. Protein extracts from these cells were generated by glass-bead lysis with vigorous agitation in co-immunoprecipitation buffer (50 mM Tris-HCl, pH 7.4, 15 mM EGTA, 100 mM NaCl, 0.2% Triton X-100, 5 mM *N*-ethylmaleimide, and phosphatase inhibitors). GST fusion proteins were purified from equal concentrations of clarified lysates by incubation with GSH-Sepharose beads (GE Healthcare). The harvested proteins were washed in co-immunoprecipitation buffer and eluted in Laemmli buffer (85). Proteins were then either resolved by SDS-PAGE and immunoblotted with α-ubiquitin and α-GST antibodies exactly as described in (22) to assess ubiquitination, or they were resolved by SDS-PAGE and stained with Coomassie Blue with the band corresponding to Aly1 or Aly2 excised for MS analyses. Proteins were excised from the gel and digested, and peptides were separated and analyzed by LC-MS/MS as described elsewhere (86). In brief, gel slices were destained with 50% acetonitrile and 25 mM ammonium bicarbonate before incubation with 10 mM DTT at 56 °C for 1 h and a 1-h incubation with 55 mM iodoacetamide to reduce and alkylate proteins. Trypsin was added to the gel pieces, and proteins were digested overnight at 37 °C. Proteolytic peptides were extracted with 70% acetonitrile and 5% formic acid, vacuum-dried, and reconstituted in 0.1% formic acid for LC-MS/MS analyses. Peptides were analyzed by nano LC-MS/MS with a Dionex HPLC system (Dionex Ultimate 3000, Thermo Fisher Scientific) interfaced with a linear ion trap MS (LTQ-XL, Thermo Fisher Scientific). Peptides were separated on a C18 column (PicoChip column, New Objective, Inc., Woburn, MA). The mass spectrometer was run in data-dependent MS/MS mode so that each full MS spectrum was followed by MS/MS scans of the eight most abundant molecular ions, and dynamic exclusion was enabled to reduce the selection of previously analyzed peptides for CID (collusion-induced dissociation). MS/MS spectra were searched against the *Saccharomyces* Genome Database using the MASCOT search engine (version 2.4.0, Matrix Science Ltd.). Oxidation of methionine and carboxyaminomethylation of cysteines were set as variable and static modifications, respectively. Identification of the results were filtered with Scaffold (Proteome Software, Portland, OR).

Inductively coupled plasma mass spectrometry

Total potassium levels in yeast cells was measured using ICP-MS. Samples for these analyses were prepared essentially as described (87, 88) with the following modifications. In brief, yeast cells containing the indicated plasmids were grown to saturation in low phosphate SC medium supplemented with 100 mM KCl. These cells were then washed in low phosphate SC medium with no KCl supplementation, inoculated at an A_{600} of 0.2 into low-phosphate SC medium supplemented with 10 mM KCl, and grown for 6–8 h, which is when the cultures reached an approximate A_{600} of 1.0. One A_{600} unit's worth of cells was then harvested by filtration on isopore membrane filters (Thermo Fisher) and washed twice in 1 μM EDTA and twice in double distilled water. The cells collected on the membrane filters were dissolved overnight in 1.5 ml of 30% nitric acid at 65 °C. Samples were then diluted 15-fold to a final concentration of 2% nitric acid, and an internal standard of beryllium, germanium, and thallium was added to all samples to evaluate signal strength and instrument drift. Sample metal concentrations were measured with a PerkinElmer NexION 300X ICP-MS, calibrated with a 5-point calibration curve. A blank sample consisting of 2% nitric acid was run after every 7–10 samples to ensure that there were no signal memory effects. At least three biological replicates were run for each sample to ensure a robust set of ICP-MS measurements.

FAP staining and confocal microscopy imaging

To assess Kir2.1-FAP localization, yeast cells containing the pRS415-*TEF1pr*-FAP-TM-Kir2.1 plasmid, where the FAP corresponded to the dL5 version of this protein motif (23, 38), were grown overnight to saturation in low-potassium SC medium supplemented with 100 mM KCl. The cells were then diluted to an A_{600} of 0.2 in low-potassium SC medium with 100 mM KCl and grown for 4–5 h at 30 °C until cells reached mid-exponential phase growth (A_{600} = 0.5–0.7). Where indicated, the cells were then treated with 200 μM LatA (Molecular Probes, Eugene, OR) or with an equal volume of DMSO vehicle for 2 h at 30 °C prior to imaging. To allow the FAP tag to fluoresce, yeast cells were next incubated with 1 μM MG-B-TAU (cell-impermeant dye) or MG-ESTER (cell-permeant dye) for 15 min at room temperature and imaged. To this end, cells were plated onto 35-mm glass-bottom microwell dishes coated with poly-D-lysine (MatTek Corp., Ashland, MA) to ensure that the yeast remained stationary. Images were acquired using a Nikon Eclipse Ti inverted microscope outfitted with a Prairie-swept field confocal scan head, an Agilent monolithic laser launch, and an Andor iXon3 camera. NIS-Elements software was used to control the imaging parameters, and all images within an experiment were captured using identical settings. Fluorescence of the FAP-bound MG-B-TAU and MG-ESTER dyes was excited using 636-nm light and the fluorescent emission was detected at 664 nm (23, 38), which was achieved using the

640-nm laser line. Maximum projections of 0.2 μm, Z-stacks through the entire cell were generated in ImageJ software (National Institutes of Health). All images within an experiment were adjusted equivalently, and an equal Unsharp Mask was applied to each image using Photoshop software (Adobe Systems Inc., San Jose, CA).

Image quantification and statistical analyses

The fluorescence intensity for all images was quantified using ImageJ software. To quantify total fluorescence with the Mg-B-TAU cell-impermeant dye, maximum projections of 0.2-μm Z-stacks through an entire cell were generated, and cells were outlined manually in ImageJ. Mean pixel intensities were measured in arbitrary units (a.u.) for each cell, and the mean background pixel intensity was subtracted. The distribution of mean pixel intensities in a.u. and the distribution of pixel intensities for each group of cells are presented as box-and-whisker plots, where the horizontal midline represents the median, the box is bounded by the upper and lower quartiles, and the whiskers denote maximal and minimal fluorescence intensities. A nonparametric Kruskal–Wallis test and Dunn's multiple-comparison post hoc analyses were performed using Prism software (GraphPad, La Jolla, CA). Statistically significant differences are indicated in the figures by *asterisks* with the associated *p* values provided in the figure legends.

Author contributions—N. A. H., C. J. K., T. D. M., A. R. K., M. P. B., D. J. B., A. F. O., and J. L. B. conceptualization; N. A. H., T. D. M., A. R. K., P. G. N., A. A. A., D. J. B., A. V. K., and A. F. O. data curation; N. A. H., C. J. K., T. D. M., A. R. K., P. G. N., A. A. A., A. D., C. S.-G., D. J. B., A. V. K., and A. F. O. formal analysis; N. A. H., M. P. B., D. J. B., A. F. O., and J. L. B. supervision; M. P. B., D. J. B., A. V. K., A. F. O., and J. L. B. funding acquisition; N. A. H., C. J. K., T. D. M., A. R. K., P. G. N., A. A. A., A. D., C. S.-G., M. P. B., and A. F. O. investigation; N. A. H. and A. F. O. visualization; N. A. H., C. J. K., T. D. M., A. R. K., P. G. N., A. A. A., A. D., C. S.-G., M. P. B., D. J. B., A. V. K., and A. F. O. methodology; N. A. H., C. J. K., T. D. M., P. G. N., and A. F. O. writing-original draft; A. F. O., and J. L. B. project administration; N. A. H., C. J. K., T. D. M., A. R. K., P. G. N., A. A. A., C. S.-G., M. P. B., D. J. B., A. V. K., A. F. O., and J. L. B. writing-review and editing.

References

1. Brette, F., and Orchard, C. (2003) T-tubule function in mammalian cardiac myocytes. *Circ. Res.* **92,** 1182–1192 CrossRef Medline
2. Curran, J., Makara, M. A., Little, S. C., Musa, H., Liu, B., Wu, X., Polina, I., Alecusan, J. S., Wright, P., Li, J., Billman, G. E., Boyden, P. A., Gyorke, S., Band, H., Hund, T. J., and Mohler, P. J. (2014) EHD3-dependent endosome pathway regulates cardiac membrane excitability and physiology. *Circ. Res.* **115,** 68–78 CrossRef Medline
3. Kolb, A. R., Needham, P. G., Rothenberg, C., Guerriero, C. J., Welling, P. A., and Brodsky, J. L. (2014) ESCRT regulates surface expression of the Kir2.1 potassium channel. *Mol. Biol. Cell* **25,** 276–289 CrossRef Medline
4. de Boer, T. P., Houtman, M. J., Compier, M., and van der Heyden, M. A. (2010) The mammalian K(IR)2.x inward rectifier ion channel family: Expression pattern and pathophysiology. *Acta Physiol.* (*Oxf.*) **199,** 243–256 Medline
5. Nichols, C. G., and Lopatin, A. N. (1997) Inward rectifier potassium channels. *Annu. Rev. Physiol.* **59,** 171–191 CrossRef Medline
6. Hibino, H., Inanobe, A., Furutani, K., Murakami, S., Findlay, I., and Kurachi, Y. (2010) Inwardly rectifying potassium channels: Their structure, function, and physiological roles. *Physiol. Rev.* **90,** 291–366 CrossRef Medline
7. Clarke, O. B., Caputo, A. T., Hill, A. P., Vandenberg, J. I., Smith, B. J., and Gulbis, J. M. (2010) Domain reorientation and rotation of an intracellular assembly regulate conduction in Kir potassium channels. *Cell* **141,** 1018–1029 CrossRef Medline
8. Plaster, N. M., Tawil, R., Tristani-Firouzi, M., Canún, S., Bendahhou, S., Tsunoda, A., Donaldson, M. R., Iannaccone, S. T., Brunt, E., Barohn, R., Clark, J., Deymeer, F., George, A. L., Jr., Fish, F. A., Hahn, A., *et al.* (2001) Mutations in Kir2.1 cause the developmental and episodic electrical phenotypes of Andersen's syndrome. *Cell* **105,** 511–519 CrossRef Medline
9. Priori, S. G., Pandit, S. V., Rivolta, I., Berenfeld, O., Ronchetti, E., Dhamoon, A., Napolitano, C., Anumonwo, J., di Barletta, M. R., Gudapakkam, S., Bosi, G., Stramba-Badiale, M., and Jalife, J. (2005) A novel form of short QT syndrome (SQT3) is caused by a mutation in the *KCNJ2* gene. *Circ. Res.* **96,** 800–807 CrossRef Medline
10. Andersen, E. D., Krasilnikoff, P. A., and Overvad, H. (1971) Intermittent muscular weakness, extrasystoles, and multiple developmental anomalies: A new syndrome? *Acta Paediatr. Scand.* **60,** 559–564 CrossRef Medline
11. Tristani-Firouzi, M., and Etheridge, S. P. (2010) Kir 2.1 channelopathies: The Andersen-Tawil syndrome. *Pflugers Arch.* **460,** 289–294 CrossRef Medline
12. Ai, T., Fujiwara, Y., Tsuji, K., Otani, H., Nakano, S., Kubo, Y., and Horie, M. (2002) Novel KCNJ2 mutation in familial periodic paralysis with ventricular dysrhythmia. *Circulation* **105,** 2592–2594 CrossRef Medline
13. Ma, D., Taneja, T. K., Hagen, B. M., Kim, B. Y., Ortega, B., Lederer, W. J., and Welling, P. A. (2011) Golgi export of the Kir2.1 channel is driven by a trafficking signal located within its tertiary structure. *Cell* **145,** 1102–1115 CrossRef Medline
14. Stockklausner, C., and Klocker, N. (2003) Surface expression of inward rectifier potassium channels is controlled by selective Golgi export. *J. Biol. Chem.* **278,** 17000–17005 CrossRef Medline
15. Yoo, D., Fang, L., Mason, A., Kim, B. Y., and Welling, P. A. (2005) A phosphorylation-dependent export structure in ROMK (Kir 1.1) channel overrides an endoplasmic reticulum localization signal. *J. Biol. Chem.* **280,** 35281–35289 CrossRef Medline
16. Nakamura, R. L., and Gaber, R. F. (1998) Studying ion channels using yeast genetics. *Methods Enzymol.* **293,** 89–104 CrossRef Medline
17. Alvaro, C. G., O'Donnell, A. F., Prosser, D. C., Augustine, A. A., Goldman, A., Brodsky, J. L., Cyert, M. S., Wendland, B., and Thorner, J. (2014) Specific α-arrestins negatively regulate *Saccharomyces cerevisiae* pheromone response by down-modulating the G-protein-coupled receptor Ste2. *Mol. Cell. Biol.* **34,** 2660–2681 CrossRef Medline
18. Becuwe, M., Vieira, N., Lara, D., Gomes-Rezende, J., Soares-Cunha, C., Casal, M., Haguenauer-Tsapis, R., Vincent, O., Paiva, S., and Léon, S. (2012) A molecular switch on an arrestin-like protein relays glucose signaling to transporter endocytosis. *J. Cell Biol.* **196,** 247–259 CrossRef Medline
19. Lin, C. H., MacGurn, J. A., Chu, T., Stefan, C. J., and Emr, S. D. (2008) Arrestin-related ubiquitin-ligase adaptors regulate endocytosis and protein turnover at the cell surface. *Cell* **135,** 714–725 CrossRef Medline
20. Nikko, E., and Pelham, H. R. (2009) Arrestin-mediated endocytosis of yeast plasma membrane transporters. *Traffic* **10,** 1856–1867 CrossRef Medline
21. Nikko, E., Sullivan, J. A., and Pelham, H. R. (2008) Arrestin-like proteins mediate ubiquitination and endocytosis of the yeast metal transporter Smf1. *EMBO Rep.* **9,** 1216–1221 CrossRef Medline
22. O'Donnell, A. F., Huang, L., Thorner, J., and Cyert, M. S. (2013) A calcineurin-dependent switch controls the trafficking function of α-arrestin Aly1/Art6. *J. Biol. Chem.* **288,** 24063–24080 CrossRef Medline
23. Szent-Gyorgyi, C., Stanfield, R. L., Andreko, S., Dempsey, A., Ahmed, M., Capek, S., Waggoner, A. S., Wilson, I. A., and Bruchez, M. P. (2013) Malachite green mediates homodimerization of antibody VL domains to form a fluorescent ternary complex with singular symmetric interfaces. *J. Mol. Biol.* **425,** 4595–4613 CrossRef Medline
24. Pratt, C. P., He, J., Wang, Y., Barth, A. L., and Bruchez, M. P. (2015) Fluorogenic green-inside red-outside (GIRO) labeling approach reveals

adenylyl cyclase-dependent control of BKα surface expression. *Bioconjug. Chem.* **26,** 1963–1971 CrossRef Medline
25. Shiwarski, D. J., Darr, M., Telmer, C. A., Bruchez, M. P., and Puthenveedu, M. A. (2017) PI3K class IIα regulates δ-opioid receptor export from the trans-Golgi network. *Mol. Biol. Cell* **28,** 2202–2219 CrossRef Medline
26. Tang, W., Ruknudin, A., Yang, W. P., Shaw, S. Y., Knickerbocker, A., and Kurtz, S. (1995) Functional expression of a vertebrate inwardly rectifying K+ channel in yeast. *Mol. Biol. Cell* **6,** 1231–1240 CrossRef Medline
27. O'Donnell, B. M., Mackie, T. D., Subramanya, A. R., and Brodsky, J. L. (2017) Endoplasmic reticulum-associated degradation of the renal potassium channel, ROMK, leads to type II Bartter syndrome. *J. Biol. Chem.* **292,** 12813–12827 CrossRef Medline
28. Tinker, A., Jan, Y. N., and Jan, L. Y. (1996) Regions responsible for the assembly of inwardly rectifying potassium channels. *Cell* **87,** 857–868 CrossRef Medline
29. Becuwe, M., and Leon, S. (2014) Integrated control of transporter endocytosis and recycling by the arrestin-related protein Rod1 and the ubiquitin ligase Rsp5. *eLife* **3,** e03307 CrossRef Medline
30. O'Donnell, A. F., Apffel, A., Gardner, R. G., and Cyert, M. S. (2010) α-Arrestins Aly1 and Aly2 regulate intracellular trafficking in response to nutrient signaling. *Mol. Biol. Cell* **21,** 3552–3566 CrossRef Medline
31. O'Donnell, A. F., McCartney, R. R., Chandrashekarappa, D. G., Zhang, B. B., Thorner, J., and Schmidt, M. C. (2015) 2-Deoxyglucose impairs *Saccharomyces cerevisiae* growth by stimulating Snf1-regulated and α-arrestin-mediated trafficking of hexose transporters 1 and 3. *Mol. Cell. Biol.* **35,** 939–955 CrossRef Medline
32. Risinger, A. L., and Kaiser, C. A. (2008) Different ubiquitin signals act at the Golgi and plasma membrane to direct GAP1 trafficking. *Mol. Biol. Cell* **19,** 2962–2972 CrossRef Medline
33. Alvarez, C. E. (2008) On the origins of arrestin and rhodopsin. *BMC Evol. Biol.* **8,** 222 CrossRef Medline
34. Picones, A., Keung, E., and Timpe, L. C. (2001) Unitary conductance variation in Kir2.1 and in cardiac inward rectifier potassium channels. *Biophys. J.* **81,** 2035–2049 CrossRef Medline
35. De Craene, J. O., Soetens, O., and Andre, B. (2001) The Npr1 kinase controls biosynthetic and endocytic sorting of the yeast Gap1 permease. *J. Biol. Chem.* **276,** 43939–43948 CrossRef Medline
36. Soetens, O., De Craene, J. O., and Andre, B. (2001) Ubiquitin is required for sorting to the vacuole of the yeast general amino acid permease, Gap1. *J. Biol. Chem.* **276,** 43949–43957 CrossRef Medline
37. Szent-Gyorgyi, C., Schmidt, B. F., Creeger, Y., Fisher, G. W., Zakel, K. L., Adler, S., Fitzpatrick, J. A., Woolford, C. A., Yan, Q., Vasilev, K. V., Berget, P. B., Bruchez, M. P., Jarvik, J. W., and Waggoner, A. (2008) Fluorogen-activating single-chain antibodies for imaging cell surface proteins. *Nat. Biotechnol.* **26,** 235–240 CrossRef Medline
38. Yan, Q., Schmidt, B. F., Perkins, L. A., Naganbabu, M., Saurabh, S., Andreko, S. K., and Bruchez, M. P. (2015) Near-instant surface-selective fluorogenic protein quantification using sulfonated triarylmethane dyes and fluorogen activating proteins. *Org. Biomol. Chem.* **13,** 2078–2086 CrossRef Medline
39. Corsi, A. K., and Schekman, R. (1996) Mechanism of polypeptide translocation into the endoplasmic reticulum. *J. Biol. Chem.* **271,** 30299–30302 CrossRef Medline
40. Preuss, D., Mulholland, J., Kaiser, C. A., Orlean, P., Albright, C., Rose, M. D., Robbins, P. W., and Botstein, D. (1991) Structure of the yeast endoplasmic reticulum: Localization of ER proteins using immunofluorescence and immunoelectron microscopy. *Yeast* **7,** 891–911 CrossRef Medline
41. Ayscough, K. R., Stryker, J., Pokala, N., Sanders, M., Crews, P., and Drubin, D. G. (1997) High rates of actin filament turnover in budding yeast and roles for actin in establishment and maintenance of cell polarity revealed using the actin inhibitor latrunculin-A. *J. Cell Biol.* **137,** 399–416 CrossRef Medline
42. Coué, M., Brenner, S. L., Spector, I., and Korn, E. D. (1987) Inhibition of actin polymerization by latrunculin A. *FEBS Lett.* **213,** 316–318 CrossRef Medline
43. Kaksonen, M., Sun, Y., and Drubin, D. G. (2003) A pathway for association of receptors, adaptors, and actin during endocytic internalization. *Cell* **115,** 475–487 CrossRef Medline
44. Hatakeyama, R., Kamiya, M., Takahara, T., and Maeda, T. (2010) Endocytosis of the aspartic acid/glutamic acid transporter Dip5 is triggered by substrate-dependent recruitment of the Rsp5 ubiquitin ligase via the arrestin-like protein Aly2. *Mol. Cell. Biol.* **30,** 5598–5607 CrossRef Medline
45. Rotin, D., Staub, O., and Haguenauer-Tsapis, R. (2000) Ubiquitination and endocytosis of plasma membrane proteins: Role of Nedd4/Rsp5p family of ubiquitin-protein ligases. *J. Membr. Biol.* **176,** 1–17 CrossRef Medline
46. Prosser, D. C., Pannunzio, A. E., Brodsky, J. L., Thorner, J., Wendland, B., and O'Donnell, A. F. (2015) α-Arrestins participate in cargo selection for both clathrin-independent and clathrin-mediated endocytosis. *J. Cell Sci.* **128,** 4220–4234 CrossRef Medline
47. Herrador, A., Léon, S., Haguenauer-Tsapis, R., and Vincent, O. (2013) A mechanism for protein monoubiquitination dependent on a trans-acting ubiquitin-binding domain. *J. Biol. Chem.* **288,** 16206–16211 CrossRef Medline
48. Kim, W., Bennett, E. J., Huttlin, E. L., Guo, A., Li, J., Possemato, A., Sowa, M. E., Rad, R., Rush, J., Comb, M. J., Harper, J. W., and Gygi, S. P. (2011) Systematic and quantitative assessment of the ubiquitin-modified proteome. *Mol. Cell* **44,** 325–340 CrossRef Medline
49. Udeshi, N. D., Mani, D. R., Eisenhaure, T., Mertins, P., Jaffe, J. D., Clauser, K. R., Hacohen, N., and Carr, S. A. (2012) Methods for quantification of *in vivo* changes in protein ubiquitination following proteasome and deubiquitinase inhibition. *Mol. Cell. Proteomics* **11,** 148–159 CrossRef Medline
50. Xu, P., Duong, D. M., Seyfried, N. T., Cheng, D., Xie, Y., Robert, J., Rush, J., Hochstrasser, M., Finley, D., and Peng, J. (2009) Quantitative proteomics reveals the function of unconventional ubiquitin chains in proteasomal degradation. *Cell* **137,** 133–145 CrossRef Medline
51. Starita, L. M., Lo, R. S., Eng, J. K., von Haller, P. D., and Fields, S. (2012) Sites of ubiquitin attachment in *Saccharomyces cerevisiae*. *Proteomics* **12,** 236–240 CrossRef Medline
52. Swaney, D. L., Beltrao, P., Starita, L., Guo, A., Rush, J., Fields, S., Krogan, N. J., and Villén, J. (2013) Global analysis of phosphorylation and ubiquitylation cross-talk in protein degradation. *Nat. Methods* **10,** 676–682 CrossRef Medline
53. Ziv, I., Matiuhin, Y., Kirkpatrick, D. S., Erpapazoglou, Z., Leon, S., Pantazopoulou, M., Kim, W., Gygi, S. P., Haguenauer-Tsapis, R., Reis, N., Glickman, M. H., and Kleifeld, O. (2011) A perturbed ubiquitin landscape distinguishes between ubiquitin in trafficking and in proteolysis. *Mol. Cell. Proteomics* **10,** M111.009753 CrossRef Medline
54. Bennett-Lovsey, R. M., Herbert, A. D., Sternberg, M. J., and Kelley, L. A. (2008) Exploring the extremes of sequence/structure space with ensemble fold recognition in the program Phyre. *Proteins* **70,** 611–625 Medline
55. Kelley, L. A., and Sternberg, M. J. (2009) Protein structure prediction on the Web: A case study using the Phyre server. *Nat. Protoc.* **4,** 363–371 CrossRef Medline
56. Albuquerque, C. P., Smolka, M. B., Payne, S. H., Bafna, V., Eng, J., and Zhou, H. (2008) A multidimensional chromatography technology for in-depth phosphoproteome analysis. *Mol. Cell. Proteomics* **7,** 1389–1396 CrossRef Medline
57. Holt, L. J., Tuch, B. B., Villén, J., Johnson, A. D., Gygi, S. P., and Morgan, D. O. (2009) Global analysis of Cdk1 substrate phosphorylation sites provides insights into evolution. *Science* **325,** 1682–1686 CrossRef Medline
58. MacGurn, J. A., Hsu, P. C., Smolka, M. B., and Emr, S. D. (2011) TORC1 regulates endocytosis via Npr1-mediated phosphoinhibition of a ubiquitin ligase adaptor. *Cell* **147,** 1104–1117 CrossRef Medline
59. Crapeau, M., Merhi, A., and André, B. (2014) Stress conditions promote yeast Gap1 permease ubiquitylation and down-regulation via the arrestin-like Bul and Aly proteins. *J. Biol. Chem.* **289,** 22103–22116 CrossRef Medline
60. Merhi, A., and André, B. (2012) Internal amino acids promote Gap1 permease ubiquitylation via TORC1/Npr1/14–3-3-dependent control of the Bul arrestin-like adaptors. *Mol. Cell. Biol.* **32,** 4510–4522 CrossRef Medline
61. Cyert, M. S., and Thorner, J. (1992) Regulatory subunit (CNB1 gene product) of yeast Ca^{2+}/calmodulin-dependent phosphoprotein phosphatases

is required for adaptation to pheromone. *Mol. Cell. Biol.* **12,** 3460–3469 CrossRef Medline
62. Shin, B. K., Wang, H., Yim, A. M., Le Naour, F., Brichory, F., Jang, J. H., Zhao, R., Puravs, E., Tra, J., Michael, C. W., Misek, D. E., and Hanash, S. M. (2003) Global profiling of the cell surface proteome of cancer cells uncovers an abundance of proteins with chaperone function. *J. Biol. Chem.* **278,** 7607–7616 CrossRef Medline
63. Prosser, D. C., Wrasman, K., Woodard, T. K., O'Donnell, A. F., and Wendland, B. (2016) Applications of pHluorin for quantitative, kinetic and high-throughput analysis of endocytosis in budding yeast. *J. Vis. Exp.* CrossRef Medline
64. Tsien, R. Y. (1998) The green fluorescent protein. *Annu. Rev. Biochem.* **67,** 509–544 CrossRef Medline
65. Mateus, C., and Avery, S. V. (2000) Destabilized green fluorescent protein for monitoring dynamic changes in yeast gene expression with flow cytometry. *Yeast* **16,** 1313–1323 CrossRef Medline
66. Boeckstaens, M., Llinares, E., Van Vooren, P., and Marini, A. M. (2014) The TORC1 effector kinase Npr1 fine tunes the inherent activity of the Mep2 ammonium transport protein. *Nat. Commun.* **5,** 3101 CrossRef Medline
67. O'Donnell, A. F. (2012) The running of the Buls: control of permease trafficking by α-arrestins Bul1 and Bul2. *Mol. Cell. Biol.* **32,** 4506–4509 CrossRef Medline
68. Foote, C., and Nothwehr, S. F. (2006) The clathrin adaptor complex 1 directly binds to a sorting signal in Ste13p to reduce the rate of its trafficking to the late endosome of yeast. *J. Cell Biol.* **173,** 615–626 CrossRef Medline
69. Valdivia, R. H., Baggott, D., Chuang, J. S., and Schekman, R. W. (2002) The yeast clathrin adaptor protein complex 1 is required for the efficient retention of a subset of late Golgi membrane proteins. *Dev. Cell* **2,** 283–294 CrossRef Medline
70. Valdivia, R. H., and Schekman, R. (2003) The yeasts Rho1p and Pkc1p regulate the transport of chitin synthase III (Chs3p) from internal stores to the plasma membrane. *Proc. Natl. Acad. Sci. U.S.A.* **100,** 10287–10292 CrossRef Medline
71. Chen, H., Kubo, Y., Hoshi, T., and Heinemann, S. H. (1998) Cyclosporin A selectively reduces the functional expression of Kir2.1 potassium channels in *Xenopus* oocytes. *FEBS Lett.* **422,** 307–310 CrossRef Medline
72. Dart, C., and Leyland, M. L. (2001) Targeting of an A kinase-anchoring protein, AKAP79, to an inwardly rectifying potassium channel, Kir2.1. *J. Biol. Chem.* **276,** 20499–20505 CrossRef Medline
73. Konig, S., Béguet, A., Bader, C. R., and Bernheim, L. (2006) The calcineurin pathway links hyperpolarization (Kir2.1)-induced Ca^{2+} signals to human myoblast differentiation and fusion. *Development* **133,** 3107–3114 CrossRef Medline
74. Helliwell, S. B., Losko, S., and Kaiser, C. A. (2001) Components of a ubiquitin ligase complex specify polyubiquitination and intracellular trafficking of the general amino acid permease. *J. Cell Biol.* **153,** 649–662 CrossRef Medline
75. Aubry, L., Guetta, D., and Klein, G. (2009) The arrestin fold: Variations on a theme. *Curr. Genomics* **10,** 133–142 CrossRef Medline
76. Hettema, E. H., Valdez-Taubas, J., and Pelham, H. R. (2004) Bsd2 binds the ubiquitin ligase Rsp5 and mediates the ubiquitination of transmembrane proteins. *EMBO J.* **23,** 1279–1288 CrossRef Medline
77. Stimpson, H. E., Lewis, M. J., and Pelham, H. R. (2006) Transferrin receptor-like proteins control the degradation of a yeast metal transporter. *EMBO J.* **25,** 662–672 CrossRef Medline
78. Gupta, R., Kus, B., Fladd, C., Wasmuth, J., Tonikian, R., Sidhu, S., Krogan, N. J., Parkinson, J., and Rotin, D. (2007) Ubiquitination screen using protein microarrays for comprehensive identification of Rsp5 substrates in yeast. *Mol. Syst. Biol.* **3,** 116 Medline
79. Ho, H. C., MacGurn, J. A., and Emr, S. D. (2017) Deubiquitinating enzymes Ubp2 and Ubp15 regulate endocytosis by limiting ubiquitination and degradation of ARTs. *Mol. Biol. Cell* **28,** 1271–1283 CrossRef Medline
80. Herrador, A., Herranz, S., Lara, D., and Vincent, O. (2010) Recruitment of the ESCRT machinery to a putative seven-transmembrane-domain receptor is mediated by an arrestin-related protein. *Mol. Cell. Biol.* **30,** 897–907 CrossRef Medline
81. Johnston, G. C., Pringle, J. R., and Hartwell, L. H. (1977) Coordination of growth with cell division in the yeast *Saccharomyces cerevisiae*. *Exp. Cell Res.* **105,** 79–98 CrossRef Medline
82. Volland, C., Galan, J. M., Urban-Grimal, D., Devilliers, G., and Haguenauer-Tsapis, R. (1994) Endocytose and degradation of the uracil permease of *S. cerevisiae* under stress conditions: Possible role of ubiquitin. *Folia Microbiol.* (*Praha*) **39,** 554–557 Medline
83. Brodsky, J. L., Hamamoto, S., Feldheim, D., and Schekman, R. (1993) Reconstitution of protein translocation from solubilized yeast membranes reveals topologically distinct roles for BiP and cytosolic Hsc70. *J. Cell Biol.* **120,** 95–102 CrossRef Medline
84. Sullivan, M. L., Youker, R. T., Watkins, S. C., and Brodsky, J. L. (2003) Localization of the BiP molecular chaperone with respect to endoplasmic reticulum foci containing the cystic fibrosis transmembrane conductance regulator in yeast. *J. Histochem. Cytochem.* **51,** 545–548 CrossRef Medline
85. Uetz, P., Giot, L., Cagney, G., Mansfield, T. A., Judson, R. S., Knight, J. R., Lockshon, D., Narayan, V., Srinivasan, M., Pochart, P., Qureshi-Emili, A., Li, Y., Godwin, B., Conover, D., Kalbfleisch, T., *et al.* (2000) A comprehensive analysis of protein-protein interactions in *Saccharomyces cerevisiae*. *Nature* **403,** 623–627 CrossRef Medline
86. Tan, R., Nakajima, S., Wang, Q., Sun, H., Xue, J., Wu, J., Hellwig, S., Zeng, X., Yates, N. A., Smithgall, T. E., Lei, M., Jiang, Y., Levine, A. S., Su, B., and Lan, L. (2017) Nek7 protects telomeres from oxidative DNA damage by phosphorylation and stabilization of TRF1. *Mol. Cell* **65,** 818–831 e815 CrossRef Medline
87. Eide, D. J., Clark, S., Nair, T. M., Gehl, M., Gribskov, M., Guerinot, M. L., and Harper, J. F. (2005) Characterization of the yeast ionome: a genome-wide analysis of nutrient mineral and trace element homeostasis in *Saccharomyces cerevisiae*. *Genome Biol.* **6,** R77 CrossRef Medline
88. Minear, S., O'Donnell, A. F., Ballew, A., Giaever, G., Nislow, C., Stearns, T., and Cyert, M. S. (2011) Curcumin inhibits growth of *Saccharomyces cerevisiae* through iron chelation. *Eukaryot. Cell* **10,** 1574–1581 CrossRef Medline
89. Brachmann, C. B., Davies, A., Cost, G. J., Caputo, E., Li, J., Hieter, P., and Boeke, J. D. (1998) Designer deletion strains derived from *Saccharomyces cerevisiae* S288C: A useful set of strains and plasmids for PCR-mediated gene disruption and other applications. *Yeast* **14,** 115–132 CrossRef Medline
90. Ko, C. H., and Gaber, R. F. (1991) TRK1 and TRK2 encode structurally related K+ transporters in *Saccharomyces cerevisiae*. *Mol. Cell. Biol.* **11,** 4266–4273 CrossRef Medline
91. Longtine, M. S., McKenzie, A., 3rd, Demarini, D. J., Shah, N. G., Wach, A., Brachat, A., Philippsen, P., and Pringle, J. R. (1998) Additional modules for versatile and economical PCR-based gene deletion and modification in *Saccharomyces cerevisiae*. *Yeast* **14,** 953–961 CrossRef Medline
92. Pagant, S., Kung, L., Dorrington, M., Lee, M. C., and Miller, E. A. (2007) Inhibiting endoplasmic reticulum (ER)-associated degradation of misfolded Yor1p does not permit ER export despite the presence of a diacidic sorting signal. *Mol. Biol. Cell* **18,** 3398–3413 CrossRef Medline
93. Winzeler, E. A., Shoemaker, D. D., Astromoff, A., Liang, H., Anderson, K., Andre, B., Bangham, R., Benito, R., Boeke, J. D., Bussey, H., Chu, A. M., Connelly, C., Davis, K., Dietrich, F., Dow, S. W., *et al.* (1999) Functional characterization of the *S. cerevisiae* genome by gene deletion and parallel analysis. *Science* **285,** 901–906 CrossRef Medline
94. Jones, E. W. (1991) Tackling the protease problem in *Saccharomyces cerevisiae*. *Methods Enzymol.* **194,** 428–453 CrossRef Medline

Select α-arrestins control cell-surface abundance of the mammalian Kir2.1 potassium channel in a yeast model

Natalie A. Hager, Collin J. Krasowski, Timothy D. Mackie, Alexander R. Kolb, Patrick G. Needham, Andrew A. Augustine, Alison Dempsey, Christopher Szent-Gyorgyi, Marcel P. Bruchez, Daniel J. Bain, Adam V. Kwiatkowski, Allyson F. O'Donnell and Jeffrey L. Brodsky

J. Biol. Chem. 2018, 293:11006-11021.
doi: 10.1074/jbc.RA117.001293 originally published online May 21, 2018

Select α-arrestins control surface abundance of the mammalian Kir2.1 potassium channel in a yeast model

Natalie A. Hager, Collin J. Krasowski, Timothy D. Mackie, Alexander R. Kolb, Patrick G. Needham, Andrew A. Augustine, Alison Dempsey, Christopher Szent-Gyorgyi, Marcel P. Bruchez, Daniel J. Bain, Adam V. Kwiatkowski, Allyson F. O'Donnell and Jeffrey L. Brodsky.

SUPPLEMENTAL MATERIALS

Supplemental Table S1. Plasmids used in this study

Plasmid	**Genotype**	**Description (Reference)**
pRS415-TEF1pr	*TEF1pr* CEN *LEU2*	(1)
pRS415-TEF1pr-Kir2.1-HA	*TEF1pr-Kir2.1-HA* CEN *LEU2*	(2)
pRS415-TEF1pr-FAP-TM-Kir2.1-HA	*TEF1pr-MFα1*$^{1-252}$*-FAP-TM-Kir2.1-HA* CEN *LEU2*	The pRS415-TEF1pr-Kir2.1-HA plasmid was used as a starting point to insert the *MFα1* (nucleotides 1-252) expressing the first 84 amino acids needed for targeting the protein to the ER. This region of *MFα1* was PCR amplified from genomic DNA using primers with *Spe*I and *Bam*HI restriction enzyme adaptors. The FAP-TM was PCR amplified from pBABE-kappa-myc-dL5-G4S-TMst plasmid (3) so that just the dL5-G4S-TM domain was contained between *Bam*HI and *Sma*I restriction enzyme site adaptors. It should be noted that the TM comes from the platelet-derived growth factor receptor. The *MFα1* and FAP-TM were cloned in frame at the N-terminus of Kir2.1. The plasmid was confirmed by sequence analyses.
pRS415-TEF1pr-Kir2.1-AAA-HA	*TEF1pr-Kir2.1*$^{GYG-AAA}$*-HA* CEN *LEU2*	(2)
pRS426-Kir2.1	*GPD1pr-Kir2.1-HA* 2 μm *URA3*	(2)
pRS425	2 μm *LEU2*	(4)
pRS425-*ALY1*	*ALY1pr-ALY1* 2 μ *LEU2*	(5)
pRS426	2 μm *URA3*	(4)
pRS426-*ALY1*	*ALY1pr-ALY1* 2 μ *URA3*	(6)
pRS426-*ALY2*	*ALY2pr-ALY2* 2 μ *URA3*	(6)
pRS426-*LDB19*	*LDB19pr-LDB19* 2 μ *URA3*	(7)
pRS426-*ROD1*	*ROD1pr-ROD1* 2 μ *URA3*	(7)
pRS426-*ROG3*	*ROG3pr-ROG3* 2 μ *URA3*	(6)
pRS426-*CSR2*	*CSR2pr-CSR2* 2 μ *URA3*	(5)
pRS426-*ECM21*	*ECM21pr-ECM21* 2 μ *URA3*	(5)
pRS426-*ART5*	*ART5pr-ART5* 2 μ *URA3*	(5)
pRS426-*ART10*	*ART10pr-ART10* 2 μ *URA3*	(5)
pRS426-*RIM8*	*RIM8pr-RIM8* 2 μ *URA3*	(5)

pRS426-*BUL1*	*BUL1pr-BUL1* 2 μ *URA3*	(5)
pRS426-*BUL2*	*BUL2pr-BUL2* 2 μ *URA3*	(5)
pRS426-*ALY1*$^{\text{PPxY-less}}$	*ALY1pr-ALY1*$^{PPxY\text{-}less}$ 2 μ *URA3*	(5)
pRS426-*ALY2*$^{\text{PPxY-less}}$	*ALY2pr-ALY2*$^{PPxY\text{-}less}$ 2 μ *URA3*	(5)
pRS426-*LDB19*$^{\text{PPxY-less}}$	*LDB19pr-LDB19*$^{PPxY\text{-}less}$ 2 μ *URA3*	(5)
pRS426-*ALY1*$^{\text{AAAAAA}}$	*ALY1pr-ALY1*^{AAAAAA} 2 μ *URA3*	(8)
pRS426-*ALY1*$^{\text{K379R}}$	*ALY1pr-ALY1*^{K379R} 2 μ *URA3*	This plasmid was made using site directed mutagenesis primers that converted the lysine at 379 to an arginine. The pRS426-*ALY1* plasmid was used as a template.
pRS426-*ALY2*$^{\text{K392R}}$	*ALY2pr-ALY2*^{K392R} 2 μ *URA3*	This plasmid was made using site directed mutagenesis primers that converted the lysine at 392 to an arginine. The pRS426-ALY1 plasmid was used as a template.
pKK212-*ALY1*	*CUP1pr-ALY1* 2μ *TRP1*	(6)
pKK212-*ALY2*	*CUP1pr-ALY1* 2μ *TRP1*	(6)
pKK212- *ALY1*$^{\text{PPxY-less}}$	*CUP1pr- ALY1*$^{\text{PPxY-less}}$ 2μ *TRP1*	pRS426-*ALY1*$^{\text{PPxY-less}}$ (5) was PCR amplified using primers that amplified the coding region of Aly1$^{\text{PPxY-less}}$ and contained *Xma*I and *Sal*I restriction enzyme adaptors. This was cloned into pKK212 to create an N-terminal, in-frame GST fusion.
pKK212- *ALY1*$^{\text{K379R}}$	*CUP1pr-ALY1*$^{\text{K379R}}$ 2μ *TRP1*	pRS426-*ALY1pr-ALY1*$^{\text{K379R}}$ (this study) was PCR amplified using primers that amplified the coding region of Aly1$^{\text{K379R}}$ and contained *Xma*I and *Sal*I restriction enzyme adaptors. This was cloned into pKK212 to create an N-terminal, in-frame GST fusion.
pKK212- *ALY2*$^{\text{PPxY-less}}$	*CUP1pr- ALY2*$^{\text{PPxY-less}}$ 2μ *TRP1*	pRS426-*ALY2*$^{\text{PPxY-less}}$ (5) was PCR amplified using primers that amplified the coding region of Aly*2*$^{\text{PPxY-less}}$ and contained *Xma*I and *Sal*I restriction enzyme adaptors. This was cloned into pKK212 to create an N-terminal, in-frame GST fusion.
pKK212-*ALY2*$^{\text{K392R}}$	*CUP1pr-ALY2*$^{\text{K392R}}$ 2μ *TRP1*	pRS426-*ALY2pr-ALY2*$^{\text{K392R}}$ (this study) was PCR amplified using primers that amplified the coding region of Aly2$^{\text{K392R}}$ and contained *Xma*I and *Sal*I restriction enzyme adaptors. This was cloned into pKK212 to create an N-terminal, in-frame GST fusion.

pRS415-*TEF1pr-SEC61-FAP*	*TEF1pr-SEC61-FAP* CEN *LEU2*	Primers containing *Bam*HI and *Hind*III restriction site adaptors were designed to amplify the coding region of Sec61, without the stop codon. The PCR product was cloned into pRS415-*TEF1pr* plasmid (1) and verified by sequence analyses. The dL5 FAP tag (3) was then PCR amplified using primers containing *Hind*II and *Sal*I restriction site adaptors and this product was cloned in frame downstream of Sec61. Plasmids were verified by sequence analyses.
pRS415-*TEF1pr-SEC63-FAP*	*TEF1pr-SEC63-FAP* CEN *LEU2*	Primers containing *Bam*HI and *Hind*III restriction site adaptors were designed to amplify the coding region of Sec61, without the stop codon. The PCR product was cloned into pRS415-*TEF1pr* plasmid (1). The dL5 FAP tag (3) was then PCR amplified using primers containing *Hind*II and *Sal*I restriction site adaptors and this product was cloned in frame downstream of Sec63. Plasmids were verified by sequence analyses.
pRS416-ZWF1pr-Kir2.1-HA	*ZWF1pr-Kir2.1-HA* CEN *URA3*	(2)

Supplemental References

1. Mumberg, D., Muller, R., and Funk, M. (1995) Yeast vectors for the controlled expression of heterologous proteins in different genetic backgrounds. *Gene* **156**, 119-122
2. Kolb, A. R., Needham, P. G., Rothenberg, C., Guerriero, C. J., Welling, P. A., and Brodsky, J. L. (2014) ESCRT regulates surface expression of the Kir2.1 potassium channel. *Molecular biology of the cell* **25**, 276-289
3. Yan, Q., Schmidt, B. F., Perkins, L. A., Naganbabu, M., Saurabh, S., Andreko, S. K., and Bruchez, M. P. (2015) Near-instant surface-selective fluorogenic protein quantification using sulfonated triarylmethane dyes and fluorogen activating proteins. *Org Biomol Chem* **13**, 2078-2086
4. Sikorski, R. S., and Hieter, P. (1989) A system of shuttle vectors and yeast host strains designed for efficient manipulation of DNA in Saccharomyces cerevisiae. *Genetics* **122**, 19-27
5. Prosser, D. C., Pannunzio, A. E., Brodsky, J. L., Thorner, J., Wendland, B., and O'Donnell, A. F. (2015) alpha-Arrestins participate in cargo selection for both clathrin-independent and clathrin-mediated endocytosis. *J Cell Sci* **128**, 4220-4234
6. O'Donnell, A. F., Apffel, A., Gardner, R. G., and Cyert, M. S. (2010) Alpha-arrestins Aly1 and Aly2 regulate intracellular trafficking in response to nutrient signaling. *Molecular biology of the cell* **21**, 3552-3566
7. Alvaro, C. G., O'Donnell, A. F., Prosser, D. C., Augustine, A. A., Goldman, A., Brodsky, J. L., Cyert, M. S., Wendland, B., and Thorner, J. (2014) Specific alpha-arrestins negatively regulate Saccharomyces cerevisiae pheromone response by down-modulating the G-protein-coupled receptor Ste2. *Molecular and cellular biology* **34**, 2660-2681
8. O'Donnell, A. F., Huang, L., Thorner, J., and Cyert, M. S. (2013) A calcineurin-dependent switch controls the trafficking function of alpha-arrestin Aly1/Art6. *The Journal of biological chemistry* **288**, 24063-24080
9. Nakamura, R. L., and Gaber, R. F. (1998) Studying ion channels using yeast genetics. *Methods Enzymol* **293**, 89-104
10. Peng, J., Schwartz, D., Elias, J. E., Thoreen, C. C., Cheng, D., Marsischky, G., Roelofs, J., Finley, D., and Gygi, S. P. (2003) A proteomics approach to understanding protein ubiquitination. *Nat Biotechnol* **21**, 921-926
11. Starita, L. M., Lo, R. S., Eng, J. K., von Haller, P. D., and Fields, S. (2012) Sites of ubiquitin attachment in Saccharomyces cerevisiae. *Proteomics* **12**, 236-240
12. Swaney, D. L., Beltrao, P., Starita, L., Guo, A., Rush, J., Fields, S., Krogan, N. J., and Villen, J. (2013) Global analysis of phosphorylation and ubiquitylation cross-talk in protein degradation. *Nat Methods* **10**, 676-682
13. Ziv, I., Matiuhin, Y., Kirkpatrick, D. S., Erpapazoglou, Z., Leon, S., Pantazopoulou, M., Kim, W., Gygi, S. P., Haguenauer-Tsapis, R., Reis, N., Glickman, M. H., and Kleifeld, O. (2011) A perturbed ubiquitin landscape distinguishes between ubiquitin in trafficking and in proteolysis. *Molecular & cellular proteomics : MCP* **10**, M111 009753

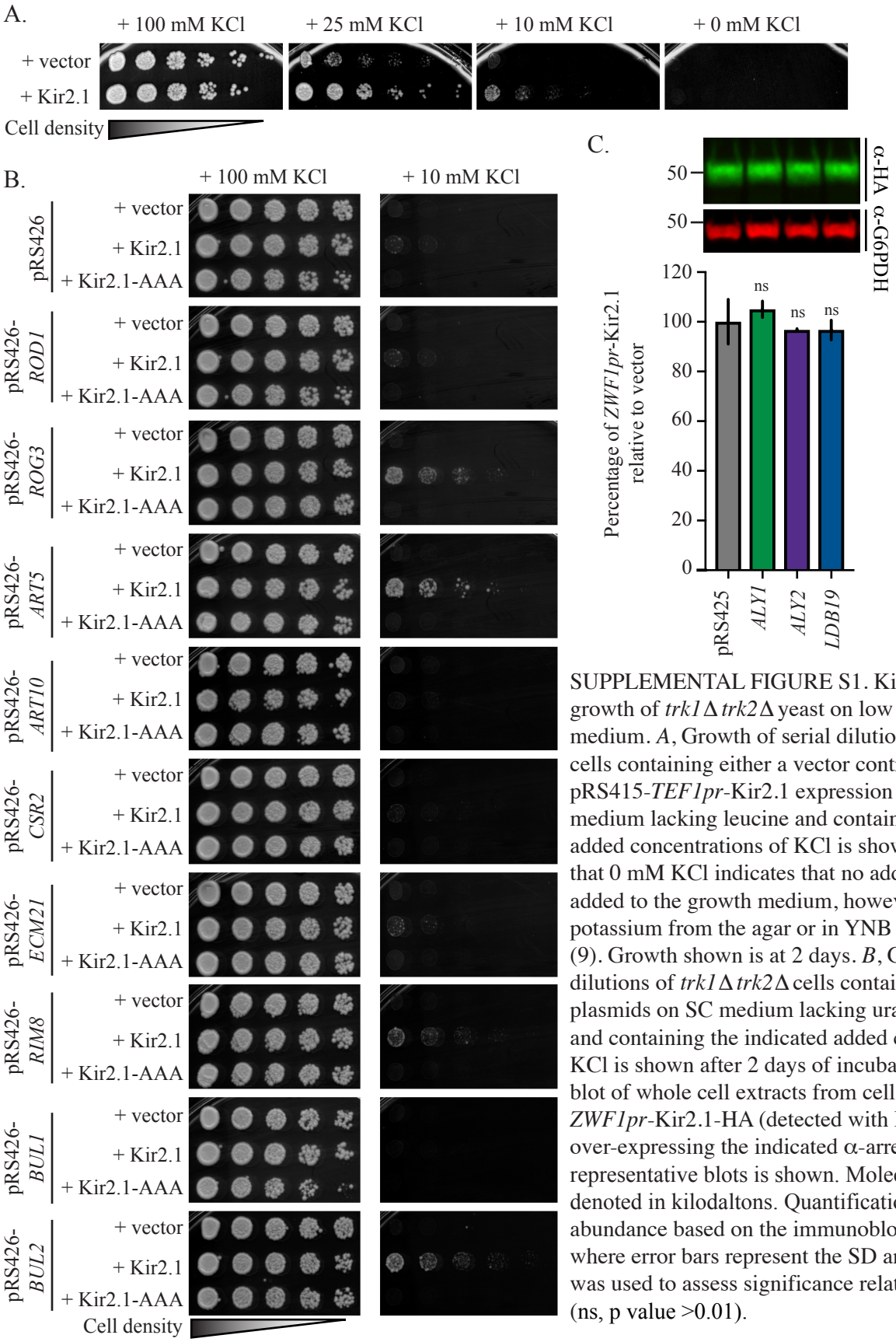

SUPPLEMENTAL FIGURE S1. Kir2.1 rescues the growth of *trk1*Δ*trk2*Δ yeast on low potassium medium. *A*, Growth of serial dilutions of *trk1*Δ*trk2*Δ cells containing either a vector control or the pRS415-*TEF1pr*-Kir2.1 expression plasmid on SC medium lacking leucine and containing the indicated added concentrations of KCl is shown. Please note that 0 mM KCl indicates that no additional KCl was added to the growth medium, however some residual potassium from the agar or in YNB powder is present (9). Growth shown is at 2 days. *B*, Growth of serial dilutions of *trk1*Δ*trk2*Δ cells containing the indicated plasmids on SC medium lacking uracil and leucine and containing the indicated added concentrations of KCl is shown after 2 days of incubation. *C*, Immunoblot of whole cell extracts from cells expressing *ZWF1pr*-Kir2.1-HA (detected with HA antibody) and over-expressing the indicated α-arrestins. One of three representative blots is shown. Molecular masses are denoted in kilodaltons. Quantification of Kir2.1-HA abundance based on the immunoblot data is shown where error bars represent the SD and a Students t-test was used to assess significance relative to the vector (ns, p value >0.01).

Supplemental Figure S1. Hager et al.

A. Aly1 amino acid sequence - 60% coverage and 152 spectra

```
   1  MLQFNTENDT VAPVFPMEQD INAAPDAVPL VQTTTLQVFV KLAEPIVFLK
  51  GFETNGLSEI APSILRGSLI VRVLKPNKLK SISITFKGIS RTEWPEGIPP
 101  KREEFSDVET VVNHTWPFYQ ADDGMNSFTL EHHSSNNSSN RPSMSDEDYL
 151  LEKSGASVYI PPTAEPPKDN SNLSLDAYER NSLSSDNLSN KPVSSDVSHD
 201  DSKLLAIQKT PLPSSSRRGS VPANFHGNSL SPHTFISDLF TKTFSNSGAT
 251  PSPEQEDNYL TPSKDSKEVF IFRPGDYIYT FEQPISQSYP ESIKANFGSV
 301  EYKLSIDIER FGAFKSTIHT QLPIKVVRLP SDGSVEETEA IAISKDWKDL
 351  LHYDVVIFSK EIVLNAFLPI DFHFAPLDKV TLHRIRIYLT ESMEYTCNSN
 401  GNHEKARRLE PTKKFLLAEH NGPKLPHIPA GSNPLKAKNR GNILLDEKSG
 451  DLVNKDFQFE VFVPSKFTNS IRLHPDTNYD KIKAHHWIKI CLRLSKKYGD
 501  NRKHFEISID SPIHILNQLC SHANTLLPSY ESHFQYCDED GNFAPAADQQ
 551  NYASHHDSNI FFPKEVLSSP VLSPNVQKMN IRIPSDLPVV RNRAESVKKS
 601  KSDNTSKKND QSSNVFASKQ LVANIYKPNQ IPRELTSPQA LPLSPITSPI
 651  LNYQPLSNSP PPDFDFDLAK RGAADSHAIP VDPPSYFDVL KADGIELPYY
 701  DTSSSKIPEL KLNKSRETLA SIEEDSFNGW SQIDDLSDED DNDGDIASGF
 751  NFKLSTSAPS ENVNSHTPIL QSLNMSLDGR KKNRASLHAT SVLPSTIRQN
 801  NQHFNDINQM LGSSDEDAFP KSQSLNFNKK LPILKINDNV IQSNSNSNNR
 851  VDNPEDTVDS SVDITAFYDP RMSSDSKFDW EVSKNHVDPA AYSVNVASEN
 901  RVLDDFKKAF REKRK*
```

B. Aly2 amino acid sequence - 56% coverage and 283 spectra

```
   1  MPMDQSISSP LFPMEKDIDI PLDATPLAQS SSLQLFIHLA EPVVFLQGFD
  51  PQKTEYPSVV LRGCLVVRIL KPTKLKSISL SFKGYSRTEW PEGIPPKRQE
 101  FVEIKDIVDH TWALYPPTEQ KSKKKMDASA PNESNNAANN FLTKESGASL
 151  YRTLSDNETI TSRKNSISGL SSLNLSPLGA PGNSSVNVKD RESRQRSRSS
 201  SVTSSNGPSR NLSPINLLKR ATSPSVSHHN YKPTTTSIFS DLLNNTFTHN
 251  DAASHHGHHI PTSSNHLAMT SNNFTSGSGG EFFVFQPGDY IYAFEELIPQ
 301  AYPESIKADF GFVEYFLFAS IERPGAFKSN ISARQVVNIV RTQAHNSVEE
 351  SEPIIISRDW ENQLYYDIVI ASKDIILDAF LPITFKFAPL DKVTLHRIRI
 401  YVTETMEYYC REKKVHRMEP TKKFLLTEQK GPKLPNLPND ANLSKAKNMG
 451  NLLQDPKNGD LVNKEYEYQI FIPSRFNNHQ QLHPDTSYEN IKANHWIKIC
 501  LRLSRVVDNK RKHYEISIDS PIHVLHRLCS HANTLLPSYD GHPASFPKET
 551  DSSISSILES SDDNINLYHN SNIFFPKEVL SSPVLSPNVQ PLDILIPHLP
 601  STSLTRNSRQ FNRNSKSHPS DNTIFNSAKL KSNIYQPESL QRELASPQAI
 651  PLSPITSPMS NMEVPPPDFD FSSDFISDAA SGTTTTEVSS SESSILPRDP
 701  PSYKDTVLHD NNQKRRPNSK HPTPPSLKAS HPNKNSDKNS SETLNKKESM
 751  SKIEENKHKR ETTPKKRENR DVKSLSTPQR EESKDSTSTG NQSNEKNRKR
 801  VLSLSSSLHS SPNNSGFAHS ALGNLSNESL RSLNRRESVQ DNLPSTIRHD
 851  NPFFTDLNQV LIEDELKNHD KNELNRHSTN TSSTPASARS SFDYSGINIS
 901  KDKLNMEPLL SKTETLTNKV NEDSFLRPND SYVDLLEPSV DTTIDITAPY
 951  ARNSSAWHPL QNDNDNNQFS PLLGSNENFL NAANAQNSAE SDHNNDIFTQ
1001  GSGLTESSKN SDSEERFISR LSSPEKVLIN TLDNESGLQS INESTL*
```

C.

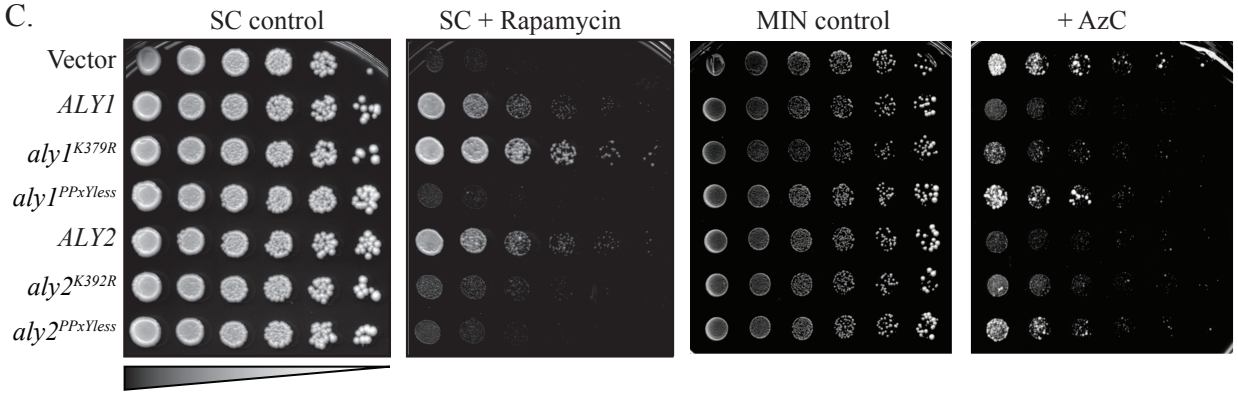

SUPPLEMENTAL FIGURE S2. Aly1 and Aly2 are ubiquitination at K379 and K392, respectively. *A and B*, The amino acid sequences of (*A*) Aly1 and (*B*) Aly2 with numbers on the left indicating amino acid position is presented. Protein sequences highlighted in grey indicate where mass spectroscopy spectra corresponding to peptides identified in our analyses. The percent coverage is indicated above the chart along with the total number of spectra mapped to either Aly1 or Aly2. Regions absent from the mass spectroscopy analysis generally lack trypsin cleavage sites or contain numerous trypsin cleavage sites, which likely generate peptides that are too long or too short, respectively, to be defined. Lysines highlighted in yellow and bold text were identified as having the diglycine mass shift associated with ubiquitination. Lysines in bold and underlined were previously identified as being modified in other ubiquitin proteomics studies (10-13). *C*, Growth of serial dilutions of BY4743 cells containing the indicated pRS426-based plasmids on SC medium lacking uracil (SC) or minimal medium containing only the amino acids required for survival (MIN) and either 500 ng/ml rapamycin or 50 μg/ml azeditidine-2-carboxylic acid (AzC). Cell growth at 4-5 days is shown.